Probing the Surface Structure of Semiconductor Nanoparticles by DNP SENS with Dielectric Support Materials

Michael P. Hanrahan,[1,2,#] Yunhua Chen,[1,2,#] Rafael Blome-Fernández,[1] Jennifer L. Stein,[3] Gregory F. Pach,[4] Marquix A. S. Adamson,[1] Nathan R. Neale,[4] Brandi M. Cossairt,[3] Javier Vela,[1,2] Aaron J. Rossini,[1,2]*

[1]Iowa State University, Department of Chemistry, Ames, IA, USA 50011
[2]US DOE Ames Laboratory, Ames, Iowa, USA, 50011
[3]University of Washington, Department of Chemistry, Seattle, WA, USA 98195
[4]Chemistry and Nanoscience Center, National Renewable Energy Laboratory, 15013 Denver West Parkway, Golden, Colorado 80401

KEYWORDS: Surface Characterization, Quantum Dots, Solid-State NMR Spectroscopy, Nanoparticles

ABSTRACT: Surface characterization is crucial for understanding how the atomic-level structure affects the chemical and photophysical properties of semiconducting nanoparticles (NPs). Solid-state nuclear magnetic resonance spectroscopy (NMR) is potentially a powerful technique for the characterization of the surface of NPs, but it is hindered by poor sensitivity. Dynamic nuclear polarization surface enhanced NMR spectroscopy (DNP SENS) has previously been demonstrated to enhance the sensitivity of surface-selective solid-state NMR experiments by one to two orders of magnitude. Established sample preparations for DNP SENS experiments on NPs require the dilution of the NPs on mesoporous silica. Using hexagonal boron nitride (*h*-BN) to disperse the NPs doubles DNP enhancements and absolute sensitivity as compared to standard protocols with mesoporous silica. Alternatively, precipitating the NPs as powders, mixing them with *h*-BN, then impregnating the powdered mixture with radical solution leads to further four-fold sensitivity enhancements by increasing the concentration of NPs in the final sample. This modified procedure provides a factor 9 improvement in NMR sensitivity as compared to previously established DNP SENS procedures, enabling challenging homonuclear and heteronuclear 2D NMR experiments on CdS, Si and Cd_3P_2 NPs. These experiments allow NMR signals from the surface, sub-surface and core sites to be observed and assigned. For example, we demonstrate that the acquisition of DNP-enhanced 2D ^{113}Cd-^{113}Cd correlation NMR experiments on CdS NPs and natural isotropic abundance 2D ^{13}C-^{29}Si HETCOR of functionalized Si NPs. These experiments provide a critical understanding of NP surface structures.

INTRODUCTION

Colloidal semiconducting nanoparticles (NPs), also referred to as quantum dots (QDs), have garnered attention in recent years for their potential in technologies such as optoelectronics,[1-2] photovoltaics,[3-5] catalysis,[6-7] biomedical sensors,[8-9] and others.[10-12] Many different synthetic methods have been employed to synthesize NPs and in general, these methods are categorized as top-down or bottom-up approaches.[13-14] NPs exhibit a wide range of functionality because their optoelectronic properties and chemical reactivity can be easily tuned by changing either the composition,[15-16] surface ligands,[17-21] and/or their size and morphology.[22-25] NPs have a high surface-to-volume ratio where different surface functional groups and surface defects strongly affect their optoelectronic and chemical properties. Therefore, obtaining a molecular level depiction of the surface of NPs is important from both a fundamental and applied perspective.

QDs are typically characterized using a variety of techniques such as Fourier transform infrared spectroscopy (FTIR), absorption and emission spectroscopies, powder X-ray diffraction (pXRD), scanning/transmission electron microscopy (SEM/TEM), and solution/solid-state nuclear magnetic resonance (NMR) spectroscopy. In general, NMR is a powerful technique for structure determination because NMR probes the local chemical environment by measuring chemical shifts or electric field gradients (EFG) and also enables the connectivity/proximity of different chemical sites to be ascertained via scalar couplings or dipolar couplings. Most of the elements found in main group inorganic semiconductors have NMR active nuclei, potentially making solid-state NMR an ideal tool for probing the structure of NPs. Solid-state NMR has previously been applied to a number of different NP systems, such as cadmium chalcogenides (CdX, X = S, Se, Te),[26-34] indium phosphide (InP),[35-37] silicon (Si),[38-42] etc.,[43-46] to determine both the surface and bulk structure. Direct excitation solid-state NMR experiments mainly probe the bulk of the NPs, although surface NMR signals are visible in small diameter NP NMR spectra.[26, 31, 35, 42-43, 45] The chemical shift of the core NMR signals is often correlated to the band gap and particle size of semiconductor NPs.[26, 31, 35, 42-43, 45] Solid-state NMR can also selectively probe the surface of inorganic NPs. Polarization transfer from the surface protons of ligands or terminating functional groups (hydride, hydroxide, etc.) to the surface hetero-nuclei enhances surface NMR signals.[47-52] Cross-polarization[53] magic angle spinning (CPMAS) is the most commonly used method to transfer polarization from protons to surface hetero-nuclei via heteronuclear dipolar couplings. CPMAS NMR spectra of NPs typically show NMR signals from both the surface and the subsurface/core layers,[29, 31, 42, 51-52, 54-55] although core NMR signals are often significantly attenuated. Alternatively, scalar polarization transfers by INEPT or *J*-HMQC enables

the selective observation of surface atoms directly bonded to H atoms[41, 56] or surface ligands.[32] For example, Noda and co-workers characterized CdSe NPs capped with ^{15}N-enriched L-cysteine and demonstrated coordination of the amine group to surface Cd atoms by measuring nitrogen-cadmium *J*-coupling constants ($^{1}J_{N\text{-}Cd}$) and ^{15}N-^{113}Cd dipolar couplings.[32]

While solid-state NMR has many potential advantages for the characterization of NPs, it is hindered by poor sensitivity which arises from low polarization of the nuclear spins, the low natural abundance of many NMR active isotopes and long longitudinal relaxation times (T_1). Surface-selective NMR experiments are also challenging because only a small fraction of the atoms constitute the surface. Consequently, long experimental times, isotopic enrichment, and/or large sample volumes are often required to obtain solid-state NMR spectra of reasonable quality that can provide meaningful structural information. For example, Strouse and co-workers were able to obtain a 2D ^{77}Se-^{1}H CP heteronuclear correlation (HETCOR) solid-state NMR spectrum of CdSe NPs that showed signals from the surface and sub-surface Se sites in close proximity to the ^{1}H nuclei of capping ligands, but the 2D HETCOR required 11 days of spectrometer time.[28]

Dynamic nuclear polarization (DNP) has been shown to greatly increase the sensitivity of solid-state NMR experiments.[57-60] In a typical DNP solid-state NMR experiment, the large spin polarization of unpaired electrons, usually from exogenous radical polarizing agents (PA), is transferred to NMR active nuclei at cryogenic temperatures (< 120 K) by irradiating the sample at a specific microwave frequency. The theoretical maximum DNP signal enhancement (ε) is proportional to the gyromagnetic ratio of the electrons and a given nucleus (maximum ε_H of 658 for protons).[59, 61] DNP solid-state NMR has previously been applied to a variety of systems including biomolecules,[62-63] pharmaceuticals,[64] polymers,[65] heterogeneous catalysts,[66-68] bulk inorganic materials,[69-71] battery materials,[72] and nanoparticles.[51-52, 55, 66, 73-80] DNP surface enhanced NMR spectroscopy (SENS) has been demonstrated as a general method to enhance NMR signals from interfaces/surfaces of inorganic materials and heterogeneous catalysts.[50, 67, 81] This technique has been primarily applied to materials such as silica and alumina which find application in heterogeneous catalysis. Typically, porous and/or high surface area inorganic materials are prepared for DNP by impregnating the solid powders with a minimal volume of solution containing a PA.

DNP SENS has previously been applied only a handful of times to colloidal semiconductor NPs. DNP was performed on colloidal solutions of metallic tin (Sn) NPs,[76] Si NPs[80] and clay NPs[82] by directly dissolving the DNP PA in the solution, then freezing the solution inside of the DNP probe. However, many colloidal NPs will precipitate when cooled to cryogenic temperatures, leading to phase segregation of the NPs and PA and poor DNP sample enhancements.[52] To address this problem Kovalenko, Copéret, Emsley and co-workers showed that colloidal NPs and PA could be impregnated onto mesoporous silica[52, 55] for DNP experiments (Figure 2A). The NPs and PA are held in close proximity to one another within the silica mesopores (or gel matrix),[79] preventing separation and resulting in significant ^{1}H DNP enhancements (ε_H> 50). However, as is shown below, there are some clear potential drawbacks of this method. First, silica is not an ideal material for DNP because it has unfavorable dielectric properties and second, the silica significantly dilutes the NPs, reducing the absolute NMR sensitivity.

Here, we demonstrate improved methods for preparing NPs for DNP-enhanced NMR experiments that yield ca. one order of magnitude improvements in absolute sensitivity as compared to established DNP sample preparation procedures. First, hexagonal boron nitride (*h*-BN) is shown to be an improved support material for dispersing NPs for DNP solid-state NMR. *h*-BN has favorable dielectric properties, (i.e. a large real component of the dielectric constant) resulting in an approximate doubling of DNP enhancements and NMR sensitivity, as compared to NP samples dispersed with mesoporous silica. It is also demonstrated that precipitated NP powders can be physically mixed with *h*-BN powder, then impregnated with PA solution, as is traditionally done for porous materials such as silica.[50] The impregnated powder procedure provides an additional large gain in sensitivity by increasing the concentration of the NPs, while still maintaining reasonably high DNP enhancements. Using these optimized sample preparation protocols, it is possible to perform 2D natural isotopic abundance homo- and hetero-nuclear correlation solid-state NMR experiments that would be impossible with conventional solid-state NMR. For example, acquisition of DNP-enhanced 2D ^{113}Cd-^{113}Cd correlation NMR experiments on CdS NPs and natural isotopic abundance 2D ^{13}C-^{29}Si HETCOR of functionalized silicon NPs is demonstrated. These 2D NMR experiments provide detailed insight into the structure and proximity of different sites on the NP surface.

RESULTS AND DISCUSSION

Testing DNP Support Materials. First, improved support materials for DNP experiments on NPs were identified.[52, 55, 79] In 2014, Kubicki *et al.* reported that the addition of materials with large real dielectric constants (refractive index) such as potassium bromide (KBr) and sapphire (α-Al_2O_3) could significantly increase DNP enhancements by improving the coupling of the microwaves to the sample.[83] Therefore, we hypothesized that DNP enhancements for dispersed NP solutions could be increased by using a support material with more favorable dielectric properties. For this purpose, materials that are free of elements typically found in semiconductor NPs were chosen to avoid introducing large background signals. Powdered hexagonal boron nitride (*h*-BN) and α-Al_2O_3 both have favorable dielectric constants[84] and will not give rise to background NMR signals for most inorganic semiconductors.

To determine the most effective support material for DNP on NPs, the proton DNP enhancement of a frozen 16 mM TEKPol 1,1,2,2-tetrachloroethane (TCE) solution was measured for different impregnated support materials. The support materials tested were *h*-BN, α-Al_2O_3, silica gel, MSU-H, and MSU-F. MSU-H and MSU-F are commercially available mesoporous silica materials with hexagonal pores and a foam morphology, respectively. Mesoporous silica was reported as the original support material for DNP solid-state NMR experiments on NPs.[52] Enough radical solution was added to each support material by impregnation so that the material appeared slightly wet.[50] A degassing step was also performed on the samples to eliminate any dissolved oxygen in the solvent and ensure optimal enhancements were achieved.[83] Consistent with previous results, the degassing step increased the ^{1}H T_1 of the radical solution and the DNP enhancements (Figure S1-S2 and Table S1). All three silica samples had solvent enhancements less than that reported for bulk TCE, consistent with previous DNP SENS experiments on silica materials (Figure 1).[67, 85-86] α-Al_2O_3 and *h*-BN gave very high solvent DNP enhancements of $\varepsilon_{C\,CP}$ = 293 and $\varepsilon_{C\,CP}$ = 357, respectively (Figure 1). Powdered α-Al_2O_3 (sapphire) is known to transmit microwaves efficiently and is the material from which DNP rotors are manufactured. The $\varepsilon_{C\,CP}$ of 357 measured for *h*-BN was the largest enhancement measured for all the support materials suggesting that *h*-

BN could be a better NP support material for DNP in comparison to mesoporous silica.

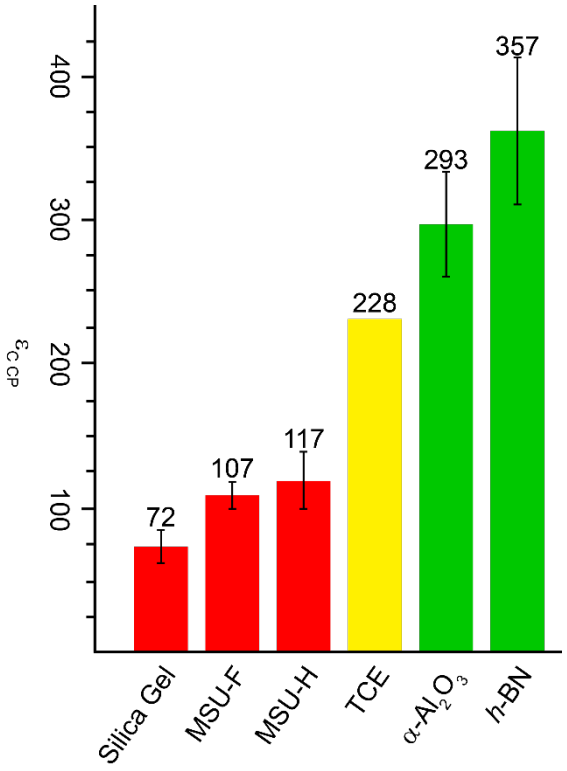

Figure 1. Comparison of the ^{13}C CPMAS DNP enhancements measured for a frozen solution of 16 mM TEKPol dissolved in 1,1,2,2-tetrachloroethane (TCE). The enhancement for the bulk frozen TCE solution was taken from Kubicki *et al.*[83] Silica gel, mesoporous silicas (MSU-F and MSU-H), alpha alumina (α-Al_2O_3) and hexagonal boron nitride (*h*-BN) were impregnated with a TEKPol TCE solution. All enhancements were determined after performing a freeze-thaw cycle inside the DNP probe, then allowing the sample to rest at the base of the probe for 5 minutes to eliminate dissolved oxygen gas prior to re-insertion.[83]

DNP Sample Preparation with h-BN Support Material. To determine the optimal NP DNP sample preparation technique, DNP-enhanced ^{13}C and ^{113}Cd solid-state NMR experiments were performed on n-decanoate capped cadmium sulfide (CdS) NPs with an average diameter of 3.1 nm determined from absorption spectroscopy[87] and TEM images (Figure S3-S4). CdS NPs were chosen for initial experiments because they are easily synthesized and air stable,[17] and the ^{13}C NMR signals of the surface ligands and ^{113}Cd NMR signals of the surface and core cadmium nuclei can be easily observed with DNP.[52,55] The first DNP NP sample preparation method tested was the previously reported impregnated support procedure,[52] but, with some slight modifications. First, 7 mg of MSU-F or 30 mg of *h*-BN were impregnated with 100 µL of a 50 mg/mL CdS NP solution in TCE. The impregnation step was performed on a balance in a fume hood and the sample mass afterward was monitored until ca. 85 µL of the TCE CdS NP solution had evaporated. The TCE was removed by evaporation to increase the concentration of NPs on the support material; if the NPs are not concentrated by evaporation of the solvent, then only ca. 1 mg of NPs will typically make it into the rotor. After evaporation, 12.5 µL of a 40 mM TEKPol TCE solution was then added to the wet powders to achieve a final radical concentration of ca. 16 mM within the TCE (Scheme S1). The impregnated MSU-F or *h*-BN powders were then transferred to the rotor. Note that the addition of about 100 µL of a 50 mg/mL CdS NP solution implies that ca. 2 - 4 mg of CdS NPs end up in the rotor; most of the rotor volume (~ 20 µL) is occupied by the solvent and support material.

^{1}H DNP enhancements were measured for the solvent and the NP surface by acquiring ^{13}C CPMAS NMR spectra with and without microwave irradiation. The DNP-enhanced ^{13}C CPMAS NMR spectra show one main observable NMR signal at 75 ppm, attributed to TCE, and signals in the at 180 ppm and the region of 30 ppm are attributed to the carbonyl and the methylene carbons of the decanoate capping ligands (Figure 2 and Figure S5). The additional two ^{13}C NMR signals at ca. 115 and 140 ppm are attributed to ligands from the cadmium precursor (Cd(9-decenyl-xanthate)$_2$). With *h*-BN as the support material, the TCE DNP enhancement ($\varepsilon_{C\,CP,\,solv}$) was double that of MSU-F, and the DNP enhancement of the NP ligand signals ($\varepsilon_{C\,CP,\,samp}$) was almost six times greater with *h*-BN (Figure S5 and Table 1). DNP-enhanced ^{1}H-^{113}Cd CP Carr-Purcell-Meiboom-Gill (CPMG) solid-state NMR spectra were also obtained for both samples to assess the absolute ^{113}Cd NMR sensitivity obtained with both support materials. All ^{113}Cd solid-state NMR spectra show three ^{113}Cd NMR signals which are attributed to the core of the CdS NP (CdS_4 sites), the surface of the CdS NP (CdS_xO_{4-x} sites) and a molecular cadmium oxide impurity (likely CdO_4 or CdO_6 sites, see detailed assignments below). The signal-to-noise ratio (SNR) of the ^{113}Cd NMR spectra and experiment time (t) were used to calculate absolute sensitivity (S, $S = \mathrm{SNR} \times t^{-1/2}$). Using *h*-BN as a support provides a 50% improvement in the ^{113}Cd NMR absolute sensitivity as compared to MSU-F as a support material (Table 1 and Figure 2). Clearly *h*-BN is a superior support material for dispersing NPs because it provides better DNP enhancements and absolute sensitivity.

Alternative sample preparation procedures were then tested to see if the concentration of NPs and absolute NMR sensitivity could be further improved. This was accomplished with a powder impregnation procedure,[50] similar to that used for DNP experiments on porous materials or microcrystalline organic solids. In the powder impregnation procedure, the NPs were first precipitated as a powder by evaporation of the colloidal solution. Then, 20 mg of precipitated NP powder was mixed with an equivalent mass of *h*-BN powder. The powders were lightly ground by hand in a mortar and pestle for less than 1 minute to evenly mix the precipitated NPs and *h*-BN. 30 mg of the mixed powder was then impregnated with 20 µL of 16 mM TEKPol TCE solution and then transferred to a sapphire rotor. The powder impregnation procedure should result in a large increase in NP concentration in the final sample as compared to the impregnated support procedure. For samples prepared with a 1:1 mass ratio of NP:*h*-BN ca. 10–15 mg of NP will make it into the rotor, corresponding to a ca. 5-fold increase in NP concentration. However, note that the NPs are likely aggregated in the impregnated powder procedure and are likely not well dispersed in the TCE or on the support (Figure 2C). If the NPs form large aggregates, then ^{1}H spin diffusion amongst the ligand hydrogen spins is likely required to distribute the DNP-enhanced ^{1}H polarization over the aggregated NPs. Consequently, the impregnated powder method is only likely to work for NPs capped with organic ligands. The presence of CdS NP aggregates on *h*-BN was confirmed with TEM of the CdS NPs prepared using the impregnated powder procedure with *h*-BN (Figure S4).

Comparing the powder impregnation and impregnated support procedures using *h*-BN as the support material, both $\varepsilon_{C\,CP,\,samp}$ and $\varepsilon_{C\,CP,\,solv}$ decrease by a factor 2 for the impregnated powders (Figure 2).

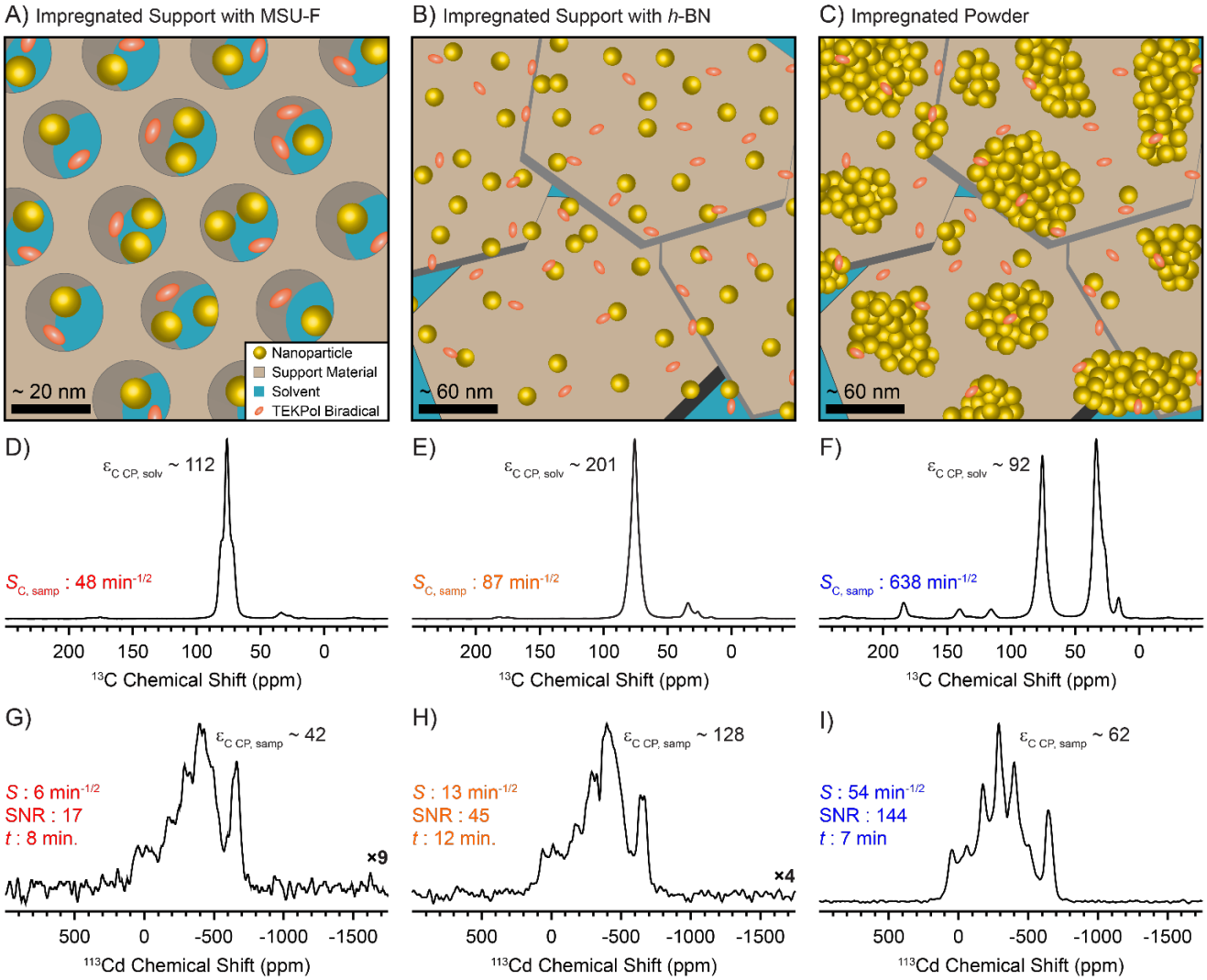

Figure 2. General schemes of the different sample preparation methods for DNP-enhanced solid-state NMR experiments on CdS NPs. The impregnated support procedure with CdS NPs and PA solution (A) dispersed inside the mesopores of silica (MSU-F) or (B) dispersed on *h*-BN. (C) The impregnated powder procedure where a mixture of CdS NP and *h*-BN were impregnated with radical solution. Yellow spheres represent CdS NPs and the orange ovals represent the radical PA. (D-F) Corresponding DNP-enhanced ^{13}C CPMAS spectra and (G-I) ^{113}Cd CP-CPMG solid-state NMR spectra of the CdS NPs showing both surface and core ^{113}Cd signals. Experiment times were between 5 and 15 min. All sample preparation methods used a final radical concentration of 16 mM TEKPol TCE and all NMR spectra were acquired with ν_{rot} = 10 kHz. ^{1}H DNP enhancements measured via ^{1}H-^{13}C CPMAS are indicated for the solvent ($\varepsilon_{C\,CP,\,solv}$) and surface ligands ($\varepsilon_{C\,CP,\,samp}$). Signal-to-noise ratio (SNR), experiment time (t) and sensitivity (S = SNR × $t^{-1/2}$) are indicated. The sample preparation schemes (A-C) are not drawn to scale and a legend for the schemes is located in the bottom right corner of A.

However, the ^{13}C and ^{113}Cd absolute NMR sensitivity increased by a factor of 7 and 4, respectively, for powder impregnation in comparison to the impregnated support procedure (Figure 2 and Table 1). It should also be noted that the ^{113}Cd NMR spectra of NPs prepared by the impregnated powder procedure show slightly sharper ^{113}Cd NMR signals than samples prepared by the impregnated support procedure. This improvement in resolution could occur because the precipitated NPs may form partially ordered aggregates while in the impregnated support sample the NPs will be dispersed in the frozen, amorphous solvent. Precipitation of the NPs may also produce changes in surface ligand concentration. In 2012 Hens and coworkers reported that 4 cycles of purification of NPs with short chain alcohols (methanol, ethanol, etc.) the surface ligand concentration went from 4.1 to 3.2 ligands•nm^{-2}, which corresponds to a 22% reduction in ligand concentration.[88] The CdS NP sample used for this study was only purified three times with a minimal amount ethanol to limit the loss of surface ligands.

The mass ratio of NP:*h*-BN used for powder impregnation was varied from 1:0 to 1:1 to determine the ideal ratio of NPs to *h*-BN that provides the best NMR sensitivity (Figure S7). A 1:1 mass ratio of NP:*h*-BN provided better absolute NMR sensitivity than a 3:1 NP:*h*-BN mass ratio or impregnation of the pure precipitated powdered NPs (1:0 CdS:*h*-BN) (Figure S7). The 1:1 sample gave 2.5 times higher DNP enhancement and 1.5 times better ^{13}C NMR sensitivity than the 1:0 sample. For comparison, the impregnated support procedure described above produces a sample which has an approximate composition of 1:5 NP:*h*-BN mass ratio. The increase in DNP enhancement with added *h*-BN could occur because *h*-BN has better dielectric characteristics and/or the *h*-BN may help reduce the size of NP aggregates. However, the increase in DNP enhancement is accompanied by dilution of the sample. Therefore, the 1:1

Table 1. DNP enhancements, experimental times, and sample sensitivities for the different DNP sample preparation procedures shown in Figure 2.

Sample Preparation Method	Impregnated Support - MSU-F	Impregnated Support - *h*-BN	Impregnated Powder
$\varepsilon_{C\,CP,\,samp}$	42	128	62
$\varepsilon_{C\,CP,\,solv}$	112	201	92
^{13}C Exp. Time (min.)	2.2	3.2	1.9
^{13}C Sample $S(min^{-1/2})^a$	48	87	637
^{113}Cd Exp. Time (min)	8.3	12.2	7.2
^{113}Cd $S(min^{-1/2})^a$	6	13	54

[a]The sensitivity (S) was calculated by dividing the signal to noise ratio by the square root of the total experiment time, $S = SNR \times t^{-1/2}$.

ratio of NP:*h*-BN likely provides the best tradeoff between DNP enhancement and NP concentration.

2D Solid-State NMR Experiments on CdS NPs. With optimal DNP sample preparation methods in hand, we were able to perform more challenging 2D correlation experiments to characterize the surface of the CdS NPs. Recently, Emsley and co-workers used DNP and 2D phase adjusted spinning sidebands enhanced by phase-incremented echo-train acquisition (2D PASS-PIETA) experiments to correlate anisotropic ^{113}Cd spinning sidebands manifolds to isotropic ^{113}Cd chemical shifts for CdSe and CdS NPs and nanoplatelets.[55] The isotropic dimension of the 2D PASS-PIETA NMR spectrum resolves the different NMR signals associated with the surface, shell and core.[55] With this in mind, the first challenging NMR experiment performed on the CdS NPs was a ^{113}Cd 2D CP magic-angle-turning (CP-MAT),[89-90] which gives similar information to a PASS-PIETA experiment (Figure 2I and Figure 3A). Note that CPMG/PIETA acquisition of the direct dimension signal was not required because of the high ^{113}Cd NMR sensitivity provided by the impregnated powder procedure. The increased sensitivity would be especially useful in cases where the transverse relaxation time is too short for CPMG/PIETA acquisition.

The 2D CP-MAT spectrum correlates the spinning sideband manifolds to the isotropic peaks in the indirect dimension. The indirect dimension shows three distinct isotropic NMR signals. The first signal occurs at an isotropic chemical shift of 52 ppm which matches the previously reported chemical shift for bulk CdS.[55, 91] Therefore, this signal corresponds to CdS_4 sites residing in the sub-surface or core regions of the CdS NPs. As expected, this site has a small chemical shift anisotropy (CSA) (Ω < 250 ppm) consistent with the highly symmetric, tetrahedral Cd coordination in the core. The second site centered at –283 ppm is assigned to the surface Cd atoms that are coordinated by the capping carboxylate ligands, in agreement with previous observations.[55] The ^{113}Cd isotropic shift of –283 ppm is intermediate between the chemical shifts of CdS (52 ppm) and molecular cadmium oxide impurity (–631 ppm), consistent with a CdS_2O_2 coordination environment. Because of the asymmetric CdS_2O_2 coordination environment, there is a large CSA of 487 ppm for this site. The ^{113}Cd chemical shift and large CSA are consistent with previously reported values for both CdS and CdSe NPs.[52, 55] Note that there is a large distribution of isotropic chemical shifts in the range of 0 to –555 ppm centered around the surface NMR signal at –283 ppm. The breadth of this distribution likely reflects the disordered nature of the surface and suggests that there could be minor numbers of Cd atoms coordinated by 1 or 3 oxygen and sulfur atoms (CdS_3O_1 and CdS_1O_3 sites). Alternatively, these signals could also arise from Cd nuclei in the sub-surface layers because bulk-like sites in the sub-surface regions may exhibit chemical shifts distinct from either surface or core NMR signals.[43] A third signal at an isotropic chemical shift of –631 ppm is also visible. This shift should correspond to Cd coordinated by 4 to 7 oxygen atoms (denoted as CdO_x sites). This site also has minimal CSA (Ω < 250 ppm), suggesting that the cadmium coordination is symmetric and possibly tetrahedral or octahedral. We hypothesize that this signal arises from a molecular cadmium impurity formed as a byproduct during the synthesis of the CdS NPs (see below).

Having identified the different Cd coordination environments present in the CdS NPs, additional 2D NMR experiments were then performed to probe the proximity/connectivity of the Cd sites. A refocused incredible natural abundance double resonance transfer experiment (refocused INADEQUATE)[92] experiment was performed to observe the connectivity of Cd species linked by bridging sulfide or oxide atoms. The INADEQUATE experiment utilizes homonuclear ^{113}Cd scalar couplings (J couplings) to generate double quantum (DQ) coherences and selectively observe ^{113}Cd spin pairs that are linked by a bridging sulfide or oxide. DQ correlations will appear in the indirect dimension at the sum of their single quantum (SQ) chemical shifts. The 2D ^{113}Cd-^{113}Cd INADEQUATE-CPMG spectrum was obtained with a J-evolution time (τ) of 2 ms, which approximately corresponds to a two-bond homonuclear cadmium J-coupling ($^2J_{Cd\text{-}Cd}$) of ca. 125 Hz (Figures 3 and S8-S9). Previously, a $^2J_{Cd\text{-}Cd}$ of 82 Hz was measured for cadmium thiolate molecular clusters with bridging sulfide ligands.[93] The ^{113}Cd-^{113}Cd 2D INADEQUATE spectrum shows a clear auto-correlation at 52 ppm in direct dimension and 104 ppm in the indirect dimension, which arises from correlations between Cd spins in the core of the CdS NPs (Figure 3). Correlations between core and surface or sub-surface Cd atoms results in a broad signal in the indirect dimension that covers a shift range of ca. 0 to –555 ppm. The broad range of chemical shifts in the indirect dimension could arise from the CSA of surface sites and/or the large range of isotropic shifts associated with surface sites. The observation of this correlation confirms the proximity of the surface and core Cd atoms. A second 2D ^{113}Cd-^{113}Cd INADEQUATE-CPMG spectrum was obtained with a mixing time of 16 ms, which approximately corresponds to a $^2J_{Cd\text{-}Cd}$ of ca. 15 Hz. This spectrum shows a single auto-correlation for the ^{113}Cd peak at –650 ppm corresponding to connections between CdO_x species, suggesting that the CdO_x impurity does not correspond to isolated molecular carboxylate compounds (Figure S9).

To determine if the CdO_x species are located in a shell around the CdS NPs or are segregated from the CdS NPs, a ^{113}Cd-^1H 2D ^1H spin diffusion HETCOR spectrum[94] with 20 ms of ^1H spin diffusion time

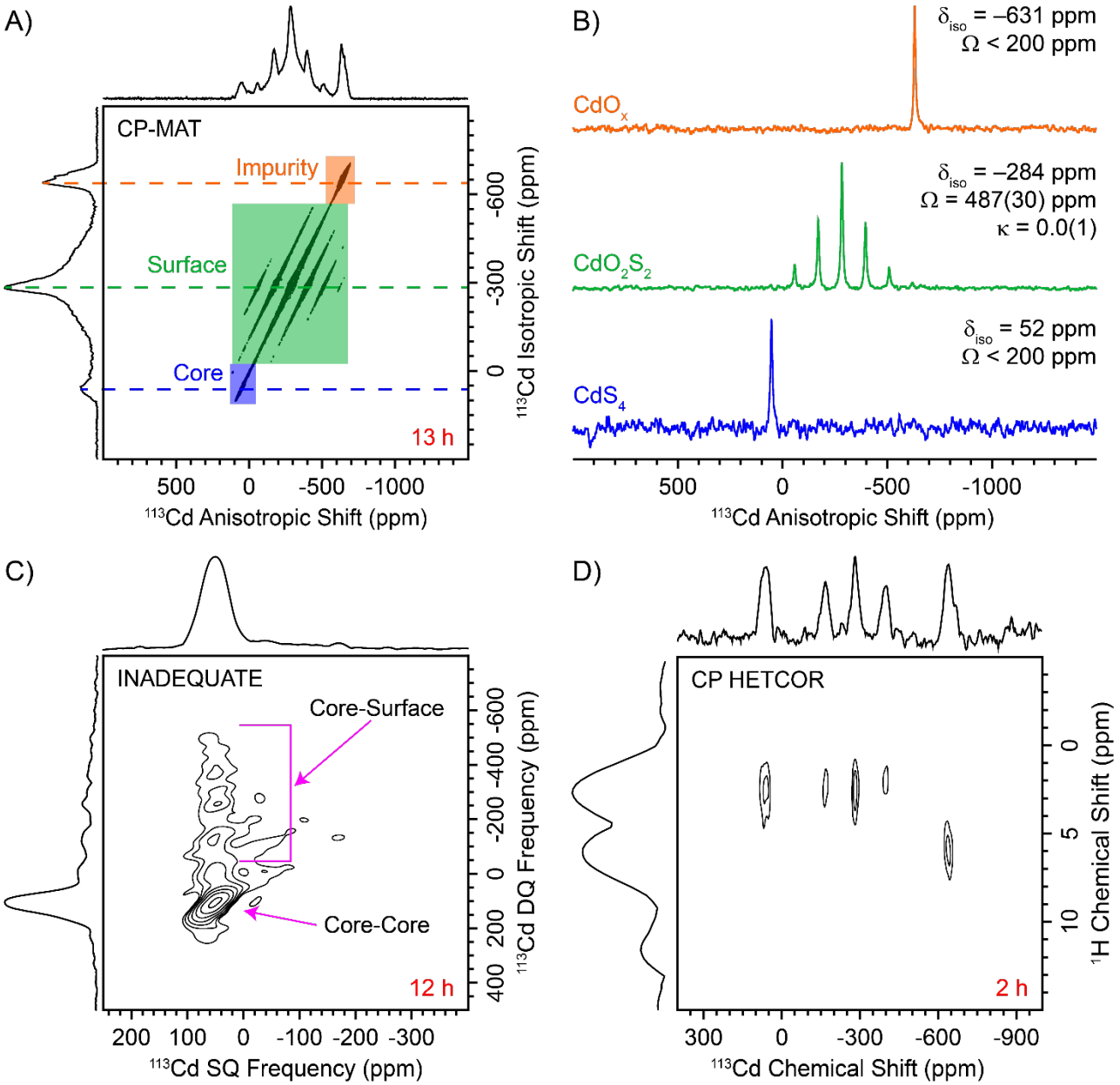

Figure 3. DNP-enhanced ^{113}Cd 2D solid-state NMR correlation spectra of CdS NPs acquired with a spinning frequency of 10 kHz. (A) 2D ^{113}Cd-^{113}Cd magic-angle turning (MAT) spectrum where the solid lines indicate distinct ^{113}Cd NMR signals. (B) Individual rows extracted from the CP-MAT 2D spectrum showing ^{113}Cd sideband manifolds associated with the core, surface and an impurity. The chemical shift tensor parameters are indicated. (C) ^{113}Cd-^{113}Cd refocused-INADEQUATE-CPMG spectrum showing correlations between core and surface ^{113}Cd sites. The diagonal line indicates autocorrelations. (D) ^{1}H spin diffusion ^{113}Cd-^{1}H CP-HETCOR acquired with 20 ms for ^{1}H spin diffusion. The CdS NP sample was prepared using the wetness impregnation sample preparation procedure.

was acquired. The spin diffusion CP-HETCOR spectrum, shows two distinct groups of ^{1}H correlations. The ^{113}Cd NMR signals from the core and surface CdS sites correlate to ^{1}H NMR signals at 2 ppm. This ^{1}H chemical shift likely corresponds to the ^{1}H spins of the decanoate capping ligands. The second correlation demonstrates that ^{113}Cd signal from the CdO_x NMR signal only correlates to a ^{1}H signal at 6.2 ppm, which likely corresponds to the ^{1}H spins of solvent (TCE). Therefore, the ^{1}H-spin diffusion CP-HETCOR experiment suggests that the ^{113}Cd NMR signals arises from a spatially segregated byproduct such as carboxylic acid hydrate compounds with bridging oxide, carboxylate or water ligands. In addition to the solid-state NMR spectroscopy, traditional NP characterization methods including transmission electron microscopy (TEM), energy dispersive X-ray spectroscopy (EDX, Figure S4) and X-ray photoelectron spectroscopy (XPS) were also applied (Figure S10 and Table S3). The EDX spectrum confirmed the presence of Cd, S, C and O within the CdS NP sample. The Cd 3*d* XPS peak position and shape confirms most Cd are in CdS and suggests the presence of cadmium coordinated by oxygen. However, since the CdS NPs are passivated with oxygen containing decanoic acid, EDX or XPS were unable to confirm domain segregations between the CdO_x and CdS particles. These results highlight the utility of solid-state NMR spectroscopy.

Finally, the proximity and ordering of the different Cd sites was also probed with ^{113}Cd spin diffusion experiments. Emsley and co-workers recently showed that homonuclear spin diffusion amongst moderate-γ nuclei such as ^{31}P, ^{119}Sn, ^{113}Cd, and ^{29}Si can relay DNP-

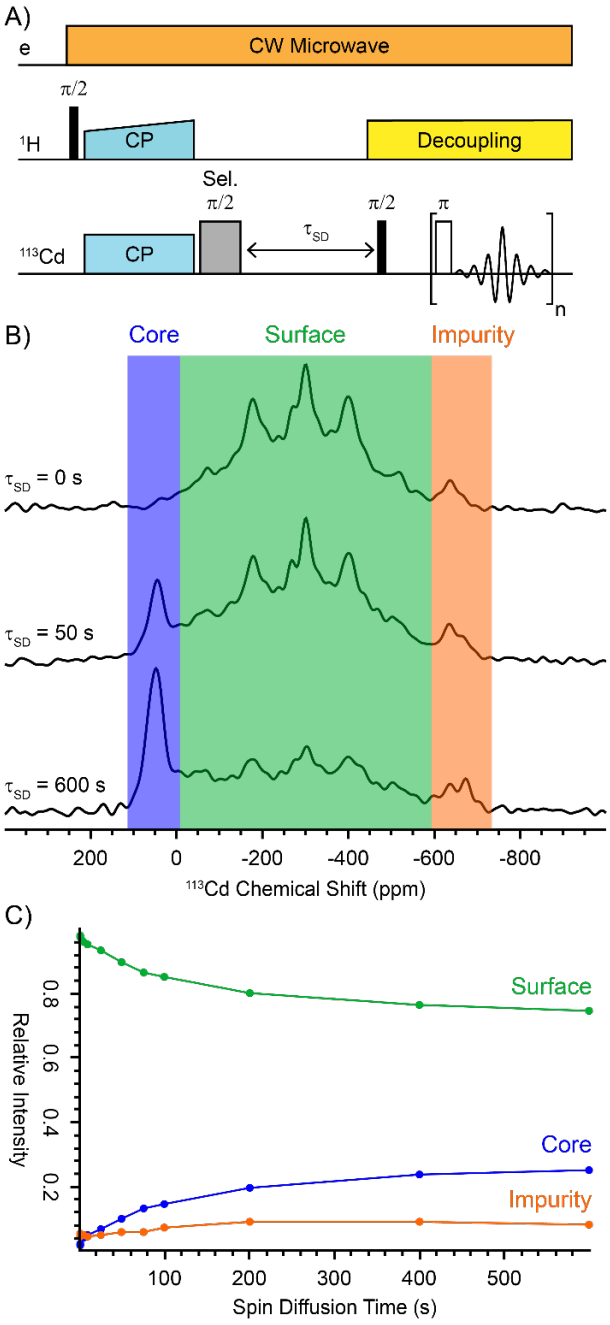

Figure 4. DNP-enhanced ^{113}Cd spin diffusion MAS NMR experiments. (A) CP spin diffusion pulse sequence with a selective 90° flip-back pulse followed by a variable ^{113}Cd spin diffusion period and CPMG signal detection. (B) ^{113}Cd CP-CPMG spin diffusion spectra with spin diffusion times of 0 s, 50 s and 600 s. (C) Intensity comparison between ^{113}Cd NMR signals for core CdS_4 (blue), surface CdS_2O_2 (green), and CdO_x (orange) as a function of ^{113}Cd spin diffusion time. In part B, the highlighted portions of the ^{113}Cd NMR spectra correspond to the regions integrated to make the plot in part C.

enhanced polarization from the surface into the core or subsurface regions of bulk inorganic materials.[70] Therefore, natural abundance ^{113}Cd spin diffusion should be observable between dipolar coupled ^{113}Cd spins within the CdS NPs. The pulse sequence for the ^{113}Cd spin diffusion experiment is shown in Figure 4A. In this experiment, ^{113}Cd magnetization is generated by CP. A frequency-selective π/2 pulse was then used to selectively store the magnetization associated with the surface sites along the *z*-axis. During longitudinal magnetization storage, all other ^{113}Cd magnetization dephases and homonuclear ^{113}Cd spin diffusion will distribute the remaining magnetization to nearby dipolar coupled ^{113}Cd spins, provided the two ^{113}Cd spins have similar chemical shifts or overlapping sidebands to permit spin diffusion.[95-97] The ^{113}Cd spin diffusion experiment clearly shows that the surface ^{113}Cd magnetization is transferred to core sites by ^{113}Cd spin diffusion (Figure 4C). No spin diffusion was observed between the surface CdS and CdO_x NMR signals, again suggesting that these sites are spatially separated. To confirm this, a second ^{113}Cd spin diffusion experiment was performed with the selective π/2 flip-back pulse applied on resonance with the CdO_x peak (Figure S11). There is no evidence of spin diffusion to the CdS surface or core NMR signals in this ^{113}Cd spin diffusion experiment. However, it is important to keep in mind that the absence of ^{113}Cd spin diffusion does not directly confirm spatial separation because overlap of ^{113}Cd NMR signals/sidebands is likely required to enable spin diffusion between different sites. Note that the 2D CP-MAT spectrum shows overlap between the CdO_x NMR signal and the last sideband associated with the CdS surface sites, suggesting spin diffusion could occur if these sites were proximate.

Cadmium Phosphide NPs. To demonstrate the generality of the improved DNP sample preparation technique it was applied to characterize other NP materials. DNP NMR was applied to characterize oleate capped cadmium phosphide NPs (Cd_3P_2) with an average diameter of 2.1 nm as measured by TEM (Figure S12). Quantum dots have been demonstrated to have high photoluminescence (PL) quantum yields and a size tunable PL over the visible and NIR spectrum, making this material ideal for LEDs and other optical applications.[98-100] The Cd_3P_2 sample was prepared with the impregnated powder method by mixing equivalent weights of *h*-BN and precipitated Cd_3P_2 NPs. Then 30 mg of the powdered mixture was impregnated with a 16 mM TEKPol TCE solution. This sample preparation gave $\varepsilon_{P\ CP} \sim 46$ (Figure 5A). All manipulations were performed in a glovebox to prevent surface oxidation. The lack of surface oxidation is confirmed by the absence of intense phosphate signals that normally appear at 0 ppm in the ^{31}P CPMAS spectrum.[37, 52, 101]

The ^{31}P CPMAS solid-state NMR spectrum of Cd_3P_2 yielded a broad ^{31}P signal centered at –300 ppm, consistent with previous reports (Figure 5A, top spectrum).[44, 99, 102] Acquisition of a ^{31}P CPMAS solid-state NMR spectrum with up to 100 s of spin diffusion time leads to the appearance of a narrower ^{31}P NMR signal at –225 ppm that is attributed to core phosphides (Figure 5A, lower spectrum). The chemical shift of the core phosphides is slightly more negative than the previously reported ^{31}P chemical shift of bulk Cd_3P_2 (peaks between –125 ppm and –175 ppm).[103] The decreased ^{31}P shift of the Cd_3P_2 NPs as compared to bulk Cd_3P_2 likely reflects the increased band gap of the NPs.[26, 35, 45]

The ^{113}Cd CP-CPMG NMR spectrum of the Cd_3P_2 shows an extremely broad NMR signal that spans 1300 ppm. Ratcliffe and coworkers previously observed that the ^{113}Cd solid-state NMR spectra of Cd_3P_2 magic-sized NPs exhibited broad spinning sideband manifolds which covered a similar chemical shift range.[44] They observed ^{113}Cd isotropic chemical shifts at +140 ppm, –243 ppm and –360 ppm.[44] The first signal was observed in a direct excitation spectrum and was attributed to core Cd NMR signals; the latter two were evident in CPMAS NMR spectra, suggesting these two NMR signals correspond to ligand coordinated surface Cd atoms.[44] A DNP-enhanced 1D CP total sideband suppression (TOSS)[104] ^{113}Cd NMR spectrum shows two very broad ^{113}Cd NMR signals centered at +220

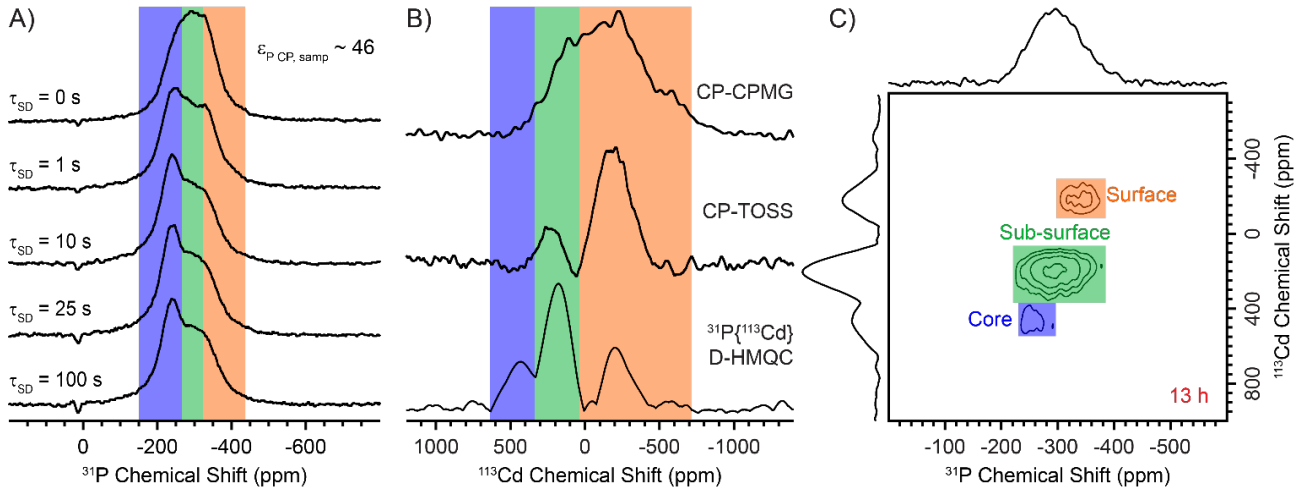

Figure 5. DNP-enhanced solid-state NMR spectra of Cd_3P_2 (A) ^{31}P CP spin echo with ^{31}P spin diffusion times from top to bottom of 0 s, 1 s, 10 s, 25 s and 100 s. (B) (top) ^{113}Cd CP-CPMG, (middle) ^{113}Cd CP-TOSS and (bottom) ^{113}Cd projection from the ^{31}P{^{113}Cd} D-HMQC. (C) 2D ^{31}P{^{113}Cd} constant time D-HMQC. All NMR spectra were acquired with a spinning frequency of 10 kHz. The highlighted regions correspond to the assigned chemical shifts of the different NMR signals: blue is assigned to the core, green is assigned to the subsurface, and orange is assigned to the surface.

ppm and –200 ppm (Figure 5B). SIMPSON[105-107] simulations confirm the sideband suppression with TOSS was sufficient for ^{113}Cd NMR signals with large CSA (Figure S13). Note that the conventional ^{113}Cd solid-state NMR spectra obtained by Ratcliffe required 4–5 days of signal averaging.[44] Here, DNP-enhanced ^{113}Cd NMR spectra were obtained in only 20 minutes.

In order to definitively assign the ^{31}P and ^{113}Cd NMR signals a ^{31}P{^{113}Cd} 2D dipolar heteronuclear multiple quantum correlation (D-HMQC) experiment was performed (Figure 5C). The ^{31}P{^{113}Cd} 2D D-HMQC spectrum shows a correlation between the core ^{31}P NMR signal at –220 ppm and ^{113}Cd NMR signal at +460 ppm that was not visible in the ^{113}Cd CP-CPMG spectrum. This ^{113}Cd NMR signal associated with the core was likely not observed in the ^{113}Cd CP-CPMG spectrum because ^{113}Cd spin diffusion is slow and thus unlikely to efficiently polarize core ^{113}Cd spins that are distant from surface ^{1}H spins. In the ^{31}P{^{113}Cd} D-HMQC experiment, ^{31}P is first polarized by CP with a 9 ms contact pulse. ^{31}P spin diffusion during the long CP contact pulse is likely fast enough to transport ^{31}P magnetization to core sites. The correlation at –350 ppm ^{31}P chemical shift and –200 ppm ^{113}Cd shift likely corresponds to surface sites since this ^{113}Cd NMR signal has the highest intensity in the surface-weighted ^{113}Cd CP-CPMG spectrum. The reduced shift of the Cd surface sites likely arises due to coordination by the carboxylate groups of the oleate capping ligands (i.e., CdO_2P_2 sites), as was observed for CdS NPs. Therefore, the remaining correlation at –280 ppm ^{31}P chemical shift and +220 ^{113}Cd chemical shift should correspond to subsurface ^{113}Cd sites.

Silicon Nanoparticles. Finally, DNP-NMR was also applied to characterize the surface of partially oxidized dodecyl functionalized silicon NPs. A particle diameter of 6.4 nm was determined from a true Voigt fit (convolution of Gaussian and Lorentzian profiles) of the Si (111) pXRD peak (Figure S14). Si NPs have a wide range of potential applications, however, the functionality of Si NPs is extremely dependent upon their surface chemistry.[11] The surface ligands of Si NPs play an important role in determining the chemical and photophysical properties of the material and also helps protect the NPs from oxidation.[11] Previously, we characterized the surface of hydride-passivated and alkyl-functionalized Si NPs using room temperature solid-state NMR with fast MAS and ^{1}H detected methods.[41]

Si NP samples were prepared for DNP by using the impregnated powder method. Powdered Si NPs and *h*-BN were mixed to give a 3:1 Si NP:*h*-BN mass ratio, then this mixture was impregnated with a 16 mM TEKPol deuterated TCE solution. Note that this sample was prepared prior to optimization of the *h*-BN:NP ratio on CdS. This procedure was performed on an air exposed sample on the bench top. Comparison of the ^{29}Si CPMAS and FTIR spectra of the air exposed Si NPs and air free Si NPs suggests that there was minimal surface oxidation (Figure S15-S16). In addition, DNP-enhanced scalar and dipolar ^{29}Si{^{1}H} HETCOR spectra confirm that the ^{29}Si NMR signal ca. –100 ppm is mainly attributed to surface hydrides (Figure S17). All Si NP spectra shown are from the air exposed Si NP sample, with the exception of the ^{29}Si CPMAS spectrum of the air free Si NP sample in Figure S15. Comparison of ^{13}C CPMAS spectra acquired with and without DNP shows that the surface ^{1}H DNP enhancement was approximately 74 (Figure 6A). This high DNP enhancement allows more challenging NMR experiments to be performed. The DNP-enhanced ^{29}Si CP-CPMG solid-state NMR spectrum was obtained in only 1 minute and is similar in appearance to the previously published room temperature ^{29}Si NMR spectrum.[41] The spectrum shows two broad NMR signals at –50 ppm and –90 ppm that correspond to silicon covalently bound to carbon (Si-R) and to surface silicon hydride species (*SiH_x) or quaternary bulk-like silicon ($SiSi_4$), respectively. There are three probable surface species that have Si–C bonds;[41] a surface silicon atom attached to an alkyl chain (***Si**R), a surface silicon monohydride with an attached alkyl chain (***Si**HR) and a trihydride species (R**Si**H_3) that is transferred to the alkyl chain during surface silylsilation with alkenes.[41]

With the use of DNP SENS, it was possible to obtain a ^{29}Si-^{29}Si 2D CP INADEQUATE spectrum in less than 4 h (Figure 6C). De Paepe and co-workers have previously demonstrated the acquisition of DNP-enhanced ^{29}Si-^{29}Si INADEQUATE spectra of alkyl functionalized silica nanoparticles.[108] They measured two bond Si-O-Si ($^{2}J_{Si\text{-}Si}$) *J*-couplings by varying the *J*-evolution time in the INADEQUATE experiments and observed optimal DQ NMR signal with τ = 14-15 ms, which corresponded to $^{2}J_{Si\text{-}Si}$ = 14 Hz (after correcting for ^{29}Si transverse relaxation).[108] Here, optimal ^{29}Si-^{29}Si INADEQUATE signal was obtained with τ = 5.6 ms, which roughly corresponds to $^{1}J_{Si\text{-}Si} \approx$ 45 Hz, which is similar to the ~ 60 Hz $^{1}J_{Si\text{-}Si}$

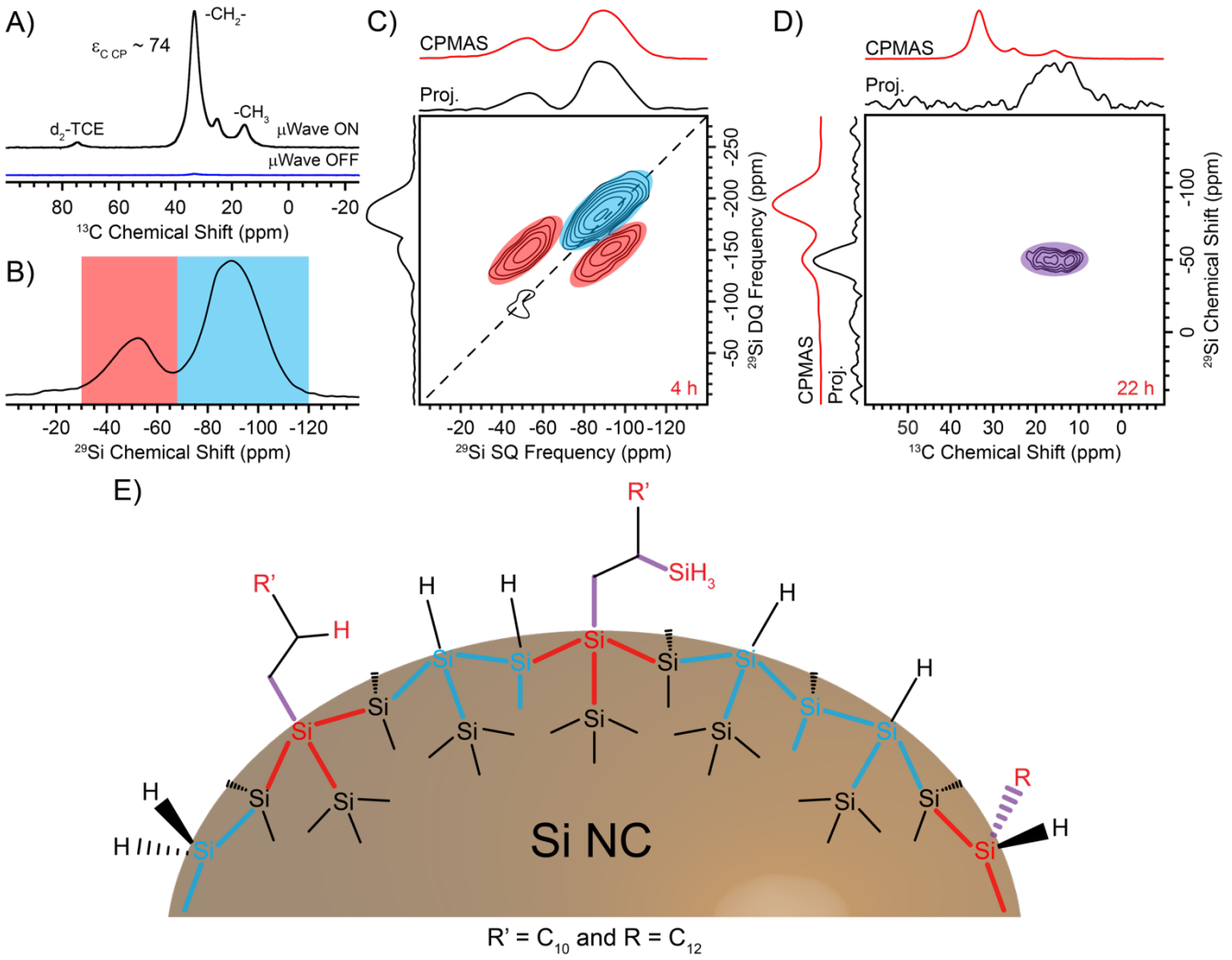

Figure 6. DNP-enhanced ^{13}C and ^{29}Si solid-state NMR spectra of air-exposed, dodecyl functionalized silicon nanocrystals at a spinning frequency of 10 kHz. (A) ^{13}C CPMAS spectra acquired with (black) and without microwave irradiation (blue). The measured DNP enhancement for the surface ligands was $\varepsilon_{C\,CP} \sim 74$. (B) ^{29}Si CP-CPMG spectrum. (C) 2D ^{29}Si-^{29}Si refocused INADEQUATE-CPMG homonuclear correlation spectrum. The diagonal line indicates autocorrelations. (D) DNP-enhanced ^{13}C-^{29}Si CP-TEDOR acquired with 3 rotor cycles of REDOR recoupling to show chemical bonded species. (E) Cartoon illustration of the different surface species and their connections. The colored bonds (purple, red and blue) indicate the different correlations observed in the 2D NMR spectra shown in (C) and (D). The sample was prepared with a 16 mM TEKPol deuterated TCE solution.

couplings reported for small molecule silanes.[109] The observed $^{1}J_{Si\text{-}Si}$ of ca. 45 Hz therefore confirms that observed ^{29}Si NMR signals arise from directly bonded silicon atoms, suggesting minimal oxidation of the surface.

The ^{29}Si INADEQUATE spectrum illustrates the structure of the Si NP (Figure 6E). The main correlation centered at –90 ppm and –175 ppm corresponds to correlations between surface hydrides (*SiH_x–*SiH_x) or between surface silicon hydrides and quaternary, bulk-like silicon (*SiH_x–$SiSi_3$). Correlations at –50 and –100 ppm in the direct dimension and –150 ppm in the indirect dimension arise from correlations between silicon atoms bonded to carbon and bulk-like silicon or surface silicon hydrides (*SiR-*SiH_x, *SiR-$SiSi_3$, *SiH_xR-*SiH_x, *SiH_xR-$SiSi_3$). Due to the overlap and similarity in the isotropic chemical shifts between *SiH_x and the subsurface atoms it is currently not possible to differentiate these possible correlations. In future experiments, ^{1}H-^{29}Si *J*- or dipole-filters will be incorporated into INADEQUATE experiments to differentiate these signals. The presence of a crystalline core of the Si NPs was confirmed with a CP spin diffusion experiment (Figure S18), which showed a sharp ^{29}Si NMR signal at chemical shift of ca. –83 ppm, consistent with prior studies.[40, 42]

DNP SENS also enabled the acquisition of a natural isotopic abundance 2D ^{13}C-^{29}Si HETCOR solid-state NMR spectrum in only 22 h (Figure 6D). To the best of our knowledge, this is the first time a ^{13}C-^{29}Si HETCOR solid-state NMR spectrum has been recorded with natural isotopic abundance. ^{13}C-^{29}Si coherence transfer was performed with the transferred-echo double resonance (TEDOR) block (Figure S19). The TEDOR NMR experiment was performed with only three-rotor cycles of rotational echo double resonance (REDOR) per recoupling block. This mixing time should selectively transfer coherence between ^{13}C bonded to ^{29}Si and suppress coherence transfer between non-bonded ^{13}C and ^{29}Si (Figure S20). The 2D ^{13}C-^{29}Si HETCOR spectrum shows correlations between the ^{29}Si signal at –50 ppm, attributed to ***Si**HR, ***Si**R and R**Si**H_3, and a broad range of ^{13}C NMR signals from 20 ppm to 10 ppm. Lee *et al.* previously obtained the ^{13}C CPMAS spectrum of Si NPs functionalized 1-

^{13}C labelled dodecene and observed similarly broad ^{13}C NMR signals.[40] The signal broadening of the 1-^{13}C signal was attributed to bonding of the alkyl chain to different facets on the Si NP surface.[40] The broad range of ^{13}C chemical shifts observed in the TEDOR spectrum could also arise because there should be carbon atoms bonded to surface silicon atoms (*Si**R** or *SiH**R**) and to silyl groups (**R**SiH_3).[41]

CONCLUSIONS

In summary, we have demonstrated improved DNP NP sample preparation procedures for DNP SENS experiments on NPs. First, for DNP NMR experiments on frozen colloidal NP solutions *h*-BN was found to be superior to silica materials. Second, the NP concentration and absolute NMR sensitivity could be substantially increased by performing experiments on precipitated NPs that were mixed with *h*-BN, then impregnated with minimal volumes of radical solution. However, as discussed above, precipitation of NPs will cause aggregation of the NPs and may alter the surface ligand concentration and/or surface structure. If aggregation is a concern then the impregnated support procedure with h-BN can still be used for experiments on dispersed NPs.

The improved NMR sensitivity enabled the acquisition of challenging 2D solid-state NMR experiments that can be used to resolve and assign the surface and core NMR signals in NPs. For CdS NPs three distinct Cd environments were observed with DNP-enhanced NMR experiments. ^{113}Cd homonuclear correlation and spin diffusion NMR experiments were used to demonstrate the proximity of the surface and core cadmium atoms in the CdS NPs and showed that a CdO_x impurity was present and separated from the CdS surface. ^{31}P spin diffusion and a ^{31}P{^{113}Cd} D-HMQC spectrum resolved distinct NMR signals associated with surface, sub-surface and core Cd and P sites within Cd_3P_2 NPs. Finally, DNP enabled acquisition of ^{29}Si-^{29}Si INADEQUATE and a ^{13}C-^{29}Si correlation spectra of function functionalized Si NPs that allow the surface bonding network to be partially resolved. We are currently using these approaches to correlate the effects of ligand exchange and other surface treatment procedures with molecular structure and photophysical properties of nanomaterials.

EXPERIMENTAL

Materials. Decanoic acid (≥98%, Aldrich), potassium tertiary butoxide (t-BuOK, 95%, Aldrich), 9-decen-1-ol (>90%, Alfa Aesar), phenyl ether (Ph_2O, 99%, Acros), carbon disulfide (CS_2, ≥99.9%, Fisher), cadmium chloride ($CdCl_2$, anhydrous, 99.995%, Strem), methanol (≥99.9%, Fisher), chloroform ($CHCl_3$, ≥99.9%, Fisher), tetrahydrofuran (THF, ≥99.9%, Fisher), diethyl ether (≥99.5%,Fisher), 1-octadecene (Aldrich), toluene (anhydrous, Aldrich), oleic acid (>99%, Aldrich), Bio-Bead S-X1 (Bio-Rad Labs), Chloroform-d ($CDCl_3$, Cambridge Isotopes Laboratories), dimethylsulfoxide-d_6 (DMSO-d_6, Cambridge Isotopes Laboratories), TEKPol biradical (Cortecnet), *h*-BN (98%, Aldrich) (Figure S21), α-Al_2O_3 (99.9%, 0.3μm grain size Aldrich), MSU-F (15 nm cell window size, Aldrich), MSU-H (7 nm pore size, Aldrich), silica gel (SiO_2, Aldrich), 1,1,2,2-tetrachloroethane (99%, Acros) and d_2 1,1,2,2-tetrachloroethane (99%, Eurisotop) were obtained from commercial suppliers and used without further purification.

Synthesis of NPs. CdS NPs. All synthesis steps were reported by Tavasoli *et al.* Specifically, 9-decen-1-ol was used as linear C10 alcohol for synthesis of xanthate precursors and decanoic acid was used as the carboxylic acid surface ligand.[17] After cooling the reaction to room temperature and dilution with chloroform (5 mL) CdS NPs were precipitated by adding a minimal amount of ethanol followed by centrifugation (4500 rpm for 10 min). The yellow residue was redissolved in a minimal amount of hexane and precipitated by ethanol and followed by centrifugation. This process was repeated once more, and the final precipitate was dried under vacuum overnight. The as-synthesized CdS NPs were precipitated without further surface modification (Figures S3 and S22-S23). The size of the CdS NPs was determined from measuring the wavelength of the first excitonic absorption peak[87] (Figure S3) and confirmed with TEM images (Figure S4) and compared to previous TEM images in which the size distribution was measured.[17] *Cd_3P_2 NPs.* All reactions for precursor and nanocrystal synthesis were run under an inert atmosphere of nitrogen using a glovebox or standard Schlenk techniques. *Warning: dimethyl cadmium is a volatile and extremely toxic reactant and was handled with care within a nitrogen glovebox. Both dimethyl cadmium and $P(SiMe_3)_3$ are pyrophoric, extremely reactive, and should be handled with caution.* Cadmium oleate and $P(SiMe_3)_3$ were prepared following literature procedures.[110] All solvents were dried over CaH_2, distilled, and stored over 4 Å molecular sieves in the a nitrogen-filled glovebox. Cadmium phosphide NPs were synthesized following a modified preparation from Eychmüller *et al.*[98] Cadmium oleate (0.55 g, 0.8 mmol), oleic acid (0.5 mL, 1.58 mmol), and 10 mL of 1-octadecene (ODE) were combined in a 25 mL 3-neck round-bottom flask under nitrogen flow on a Schlenk line and heated to 150 °C while stirring. $P(SiMe_3)_3$ (60 μL, 0.2 mmol) in 1 mL of ODE was rapidly injected into the flask. After 3 min, the solution was cooled down by placing the flask in an oil bath. Particles were isolated by first removing the ODE through distillation under reduced pressure, resuspending the resulting paste in 2 mL of toluene, and centrifuging for 10 min at 7,000 rpm. Insoluble products were removed, and the NP solution was purified by gel permeation chromatography to remove excess free ligand (Figure S24) Powdered NP samples were obtained by removing the toluene under a vacuum. *Si NPs.* Powdered alkyl-functionalized Si NPs (from radical-initiated reaction of hydride-terminated Si NPs with 1-dodecene) were prepared following our established procedures[41, 111-112] and exposed to air for several days prior to preparing the sample for DNP (Figure S16). The Si NP particle diameter was estimated to be 6.4 nm from pXRD (Figure S14), consistent with our prior extensive characterization of particle size by TEM and correlation with emission peak energy.[111]

DNP sample preparations. Impregnated support procedure. 30 mg of *h*-BN, or 7 mg of MSU-F were massed out on a balance. The difference in the required amount of h-BN or MSU-F reflects differences in density and surface areas. The support materials were then impregnated with 100 μL of a 50 mg/mL concentration of CdS NPs in (TCE) in the fume hood. The NP solution was then evaporated down to 20 μL on the balance in the fume hood. Next 10 μL of 40 mM TEKPol TCE solution was added to achieve a final radical concentration ca. 16 mM. Once the radical solution was added to the sample it was then packed into a DNP 3.2 mm sapphire rotor (Scheme S1).

Incipient wetness impregnation procedure. 20 mg of *h*-BN and 20 mg of powdered NPs (CdS or Cd_3P_2) were weighed out and added to a mortar and pestle and were gently ground for ca. 1 min to mix the NPs and support material. 30 mg of the powder mixture was then added to a watch glass where 20 μL of a 16 mM TEKPol TCE solution was added. After the addition of the radical solution the sample was then packed into a DNP 3.2 mm sapphire rotor (Scheme S2). The sample preparation for the Si NPs was similar to the above method however 10 mg of h-BN and 30 mg of Si NPs was used to

make the powder mixture and 16 mM TEKPol in deuterated TCE was used for the impregnation step. The Cd_3P_2 NPs were prepared in glovebox to prevent oxidation.

Optical Absorption Characterization of CdS NPs. Absorption spectra were measured with a photodiode-array Agilent 8453 UV–vis spectrophotometer. Solvent absorption was subtracted from all spectra. Steady-state photoluminescence (PL) spectra were measured with a Horiba-Jobin Yvon Nanolog scanning spectrofluorometer equipped with a photomultiplier detector. *Cd_3P_2 NPs.* Absorption spectra were collected in a quartz cuvette using a Cary 5000 UV-Vis spectrometer from Agilent. Fluorescence measurements were taken on a Horiba Jobin Yvon FluoroMax-4 fluorescence spectrometer.

CdS solution NMR. Solution ^{1}H NMR spectra were obtained with a 9.4 T Varian MR-400 spectrometer equipped with a OneNMR pulse-field-gradient probe. All solution ^{1}H NMR spectra were obtained using a pulse acquire pulse sequence, with 32 transients and a recycle delay of 1 s.

TEM and EDX. CdS NPs. TEM and EDX point analysis was performed on carbon coated copper grids using a FEI Tecnai G2-F20 scanning transmission electron microscope (STEM) at the Ames Laboratory Sensitive Instrument Facility. *Cd_3P_2 NPs.* TEM characterization was performed on a FEI Tecnai G2 F20 microscope at an accelerating voltage of 200 kV at the Molecular Engineering and Sciences Institute (University of Washington, Seattle). The size distributions of the NPs were determined by manual measurement of TEM images using the software ImageJ.

XPS characterization of CdS NPs. XPS measurements were performed using a Kratos Amicus/ESCA 3400 instrument. The sample was irradiated with 240 W unmonochromated Mg Kα X-rays, and photoelectrons emitted at 0° from the surface normal were energy analyzed using a DuPont type analyzer. The pass energy was set at 150 eV. CasaXPS was used to process raw data files. XPS spectra were energy calibrated to the C 1s peak position at 284.6 eV.

FTIR characterization of Si NPs. FTIR absorbance measurements were made on a Bruker Alpha FTIR spectrometer using a diffuse reflectance infrared Fourier transform spectrometer (DRIFTS) attachment with a resolution of 4 cm^{-1}. Reflective gold-coated polish Si wafers were used as the substrate for the measurement. A background measurement was taken using a bare substrate and then the Si NPs were deposited by drop casting from toluene. Samples were dried on a hotplate at 100°C in an Ar atmosphere for 10 min. Spectra were baseline-corrected using the concave rubberband correction method (2 iterations).

DNP solid-state NMR measurements. DNP NMR experiments were acquired on a Bruker 9.4 T 400 MHz/ 263 GHz Bruker solid-state NMR/ gyrotron equipped with an AVANCE III console. A Bruker 3.2 mm triple resonance probe was configured in ^{1}H-X mode capable of tuning from ^{13}C to ^{113}Cd for CdS NPs. For the Si NPs the DNP 3.2 mm triple resonance probe was configured to ^{1}H-^{13}C-^{29}Si and for the Cd_3P_2 NPs the probe was configured to ^{1}H-^{31}P-^{113}Cd. The radiofrequency (rf) pulses for ^{1}H and ^{13}C were calibrated using DNP-enhanced TCE NMR signals. ^{113}Cd rf pulses were calibrated on molecular cadmium xanthate (the cadmium precursor for synthesis of CdS NPs). Both ^{31}P and ^{29}Si rf pulses were calibrated directly on the samples. Samples were packed into DNP sapphire 3.2 mm (outer diameter) rotors with teflon inserts and zirconia drive caps. All samples were spun at 10 kHz and the sample temperatures were ~110 K. The error bars were determined for the enhancement measurements in Figure 1 by measuring the SNR of the spectra recorded with and without microwaves. One standard deviation in the signal intensities (σ) was assumed to equal to SNR multiplied by peak amplitudes. Using standard propagation of error formulas we then calculated 3σ for each enhancement measurement. ^{1}H chemical shifts were referenced to neat tetramethylsilane through the use of TCE ($\delta_{iso}(^1H) = 6.2$ ppm) as a secondary chemical shift standard. Previously published relative NMR frequencies were used to indirectly reference the ^{31}P, ^{13}C, ^{113}Cd and ^{29}Si chemical shifts.[113] The CP spin-echo, CP-TOSS,[104] CP-CPMG,[114] CP-MAT,[89] refocused-INADEQUATE[92] and CP spin diffusion,[70] CP-TEDOR,[115] constant time[116] CP-D-HMQC[117] and INEPT HETCOR[118] experiments were performed with previously published pulse sequences. The refocused-INADEQUATE pulse sequence was modified to incorporate CPMG signal detection. In both CP-TEDOR and CP-D-HMQC pulse sequences dipolar recoupling was performed with a REDOR scheme[119] where recoupling pulses were centered at one-quarter and three-quarters of the rotor cycle. The REDOR recoupling pulses were phase cycled with the XY-8 scheme[120] to compensate for offsets and pulse imperfections. During acquisition all experiments utilized SPINAL-64[121] for ^{1}H heteronuclear decoupling with a 100 kHz ^{1}H rf field. For a more detailed explanation of the solid-state NMR experiments performed please see the SI.

ASSOCIATED CONTENT

Additional Supplementary information including experimental details, Tables and Figures of NMR spectra is located in the supplemental information.

AUTHOR INFORMATION

Author Contributions

#These authors contributed equally.

Corresponding Author

*(AJR) E-mail: arossini@iastate.edu, Phone: 515-294-8952

ACKNOWLEDGMENT

DNP-NMR experiments, CdS synthesis and data interpretation and analysis (MPH, YC and AJR) was supported by the U.S. Department of Energy (DOE), Office of Science, Basic Energy Sciences, Materials Science and Engineering Division. The Ames Laboratory is operated for the U.S. DOE by Iowa State University under contract # DE-AC02-07CH11358. Synthesis of Cd_3P_2 NPs (JLC and BMC) was supported by the U.S. National Science Foundation grant CHE-1552164 and the David and Lucile Packard Foundation. This work was authored in part by employees of the Alliance for Sustainable Energy LLC, the manager and operator of the National Renewable Energy Laboratory for the U.S. DOE under contract No. DE-AC36-08GO28308. Silicon nanoparticle synthesis, surface functionalization, infrared spectroscopy, and some data interpretation (GFP and NRN) was funded by the U.S. DOE, Office of Science, Office of Basic energy Sciences, Division of Chemical Sciences, Geosciences and Biosciences, Solar Photochemistry Program. JV acknowledges support from the U.S. National Science Foundation for a grant from the Division of Chemistry, Macromolecular, Supramolecular and Nanochemistry program (1905066). XPS work of CdS NPs was performed at the Materials Analysis and Research Laboratory of the ISU Office of Biotechnology. Electron microscopy of CdS NPs was performed at the Sensitive Instrument Facility of the Ames Laboratory, which is operated for the U.S. Department of Energy by Iowa State University under Contract No. DE-AC02-07CH11358. Electron microscopy of Cd_3P_2 NPs was performed at the Molecular Analysis Facility, a

National Nanotechnology Coordinated Infrastructure site at the University of Washington which is supported in part by the National Science Foundation (grant NNCI-1542101), the University of Washington, the Molecular Engineering & Sciences Institute, and the Clean Energy Institute. We thank Dr. Tian Wei Goh and Prof. Wenyu Huang for measuring the BET surface area of *h*-BN. We thank Dr. Dapeng Jing for assistance with XPS spectroscopy of the CdS NPs and Dr. Max Friedfeld for obtaining TEM images of Cd_3P_2 NPs.

REFERENCES

1. Cao, A. N.; Liu, Z.; Chu, S. S.; Wu, M. H.; Ye, Z. M.; Cai, Z. W.; Chang, Y. L.; Wang, S. F.; Gong, Q. H.; Liu, Y. F., A Facile One-step Method to Produce Graphene-CdS Quantum Dot Nanocomposites as Promising Optoelectronic Materials. *Adv. Mater.* **2010,** *22*, 103-106.

2. Pan, J.; Quan, L. N.; Zhao, Y. B.; Peng, W.; Murali, B.; Sarmah, S. P.; Yuan, M. J.; Sinatra, L.; Alyami, N. M.; Liu, J. K.; Yassitepe, E.; Yang, Z. Y.; Voznyy, O.; Comin, R.; Hedhili, M. N.; Mohammed, O. F.; Lu, Z. H.; Kim, D. H.; Sargent, E. H.; Bakr, O. M., Highly Efficient Perovskite-Quantum-Dot Light-Emitting Diodes by Surface Engineering. *Adv. Mater.* **2016,** *28*, 8718-8725.

3. Gunes, S.; Fritz, K. P.; Neugebauer, H.; Sariciftci, N. S.; Kumar, S.; Scholes, G. D., Hybrid Solar Cells using PbS Nanoparticles. *Sol. Energy Mater. Sol. Cells* **2007,** *91*, 420-423.

4. Couderc, E.; Greaney, M. J.; Brutchey, R. L.; Bradforth, S. E., Direct Spectroscopic Evidence of Ultrafast Electron Transfer from a Low Band Gap Polymer to CdSe Quantum Dots in Hybrid Photovoltaic Thin Films. *J. Am. Chem. Soc.* **2013,** *135*, 18418-18426.

5. Crisp, R. W.; Panthani, M. G.; Rance, W. L.; Duenow, J. N.; Parilla, P. A.; Callahan, R.; Dabney, M. S.; Berry, J. J.; Talapin, D. V.; Luther, J. M., Nanocrystal Grain Growth and Device Architectures for High-Efficiency CdTe Ink-Based Photovoltaics. *ACS Nano* **2014,** *8*, 9063-9072.

6. Zhao, J.; Holmes, M. A.; Osterloh, F. E., Quantum Confinement Controls Photocatalysis: A Free Energy Analysis for Photocatalytic Proton Reduction at CdSe Nanocrystals. *ACS Nano* **2013,** *7*, 4316-4325.

7. Yu, X. L.; Shavel, A.; An, X. Q.; Luo, Z. S.; Ibanez, M.; Cabot, A., Cu2ZnSnS4-Pt and Cu2ZnSnS4-Au Heterostructured Nanoparticles for Photocatalytic Water Splitting and Pollutant Degradation. *J. Am. Chem. Soc.* **2014,** *136*, 9236-9239.

8. He, X. W.; Ma, N., An Overview of Recent Advances in Quantum Dots for Biomedical Applications. *Colloids Surf., B* **2014,** *124*, 118-131.

9. Xu, G.; Zeng, S.; Zhang, B.; Swihart, M. T.; Yong, K.-T.; Prasad, P. N., New Generation Cadmium-Free Quantum Dots for Biophotonics and Nanomedicine. *Chem. Rev.* **2016,** *116*, 12234-12327.

10. Kovalenko, M. V.; Manna, L.; Cabot, A.; Hens, Z.; Talapin, D. V.; Kagan, C. R.; Klimov, V. I.; Rogach, A. L.; Reiss, P.; Milliron, D. J.; Guyot-Sionnnest, P.; Konstantatos, G.; Parak, W. J.; Hyeon, T.; Korgel, B. A.; Murray, C. B.; Heiss, W., Prospects of Nanoscience with Nanocrystals. *ACS Nano* **2015,** *9*, 1012-1057.

11. Dasog, M.; Kehrle, J.; Rieger, B.; Veinot, J. G., Silicon Nanocrystals and Silicon-Polymer Hybrids: Synthesis, Surface Engineering, and Applications. *Angew. Chem. Int. Ed.* **2016,** *55*, 2322-2339.

12. Zhou, W.; Coleman, J. J., Semiconductor Quantum Dots. *Curr. Opin. Solid State Mater. Sci.* **2016,** *20*, 352-360.

13. Bera, D.; Qian, L.; Tseng, T. K.; Holloway, P. H., Quantum Dots and Their Multimodal Applications: A Review. *Materials* **2010,** *3*, 2260-2345.

14. Ruberu, T. P. A.; Albright, H. R.; Callis, B.; Ward, B.; Cisneros, J.; Fan, H. J.; Vela, J., Molecular Control of the Nanoscale: Effect of Phosphine-Chalcogenide Reactivity on CdS-CdSe Nanocrystal Composition and Morphology. *ACS Nano* **2012,** *6*, 5348-5359.

15. Bailey, R. E.; Nie, S. M., Alloyed Semiconductor Quantum Dots: Tuning the Optical Properties without Changing the Particle Size. *J. Am. Chem. Soc.* **2003,** *125*, 7100-7106.

16. Vela, J., Molecular Chemistry to the Fore: New Insights into the Fascinating World of Photoactive Colloidal Semiconductor Nanocrystals. *J. Phys. Chem. Lett.* **2013,** *4*, 653-668.

17. Tavasoli, E.; Guo, Y. J.; Kunal, P.; Grajeda, J.; Gerber, A.; Vela, J., Surface Doping Quantum Dots with Chemically Active Native Ligands: Controlling Valence without Ligand Exchange. *Chem. Mater.* **2012,** *24*, 4231-4241.

18. Buckley, J. J.; Couderc, E.; Greaney, M. J.; Munteanu, J.; Riche, C. T.; Bradforth, S. E.; Brutchey, R. L., Chalcogenol Ligand Toolbox for CdSe Nanocrystals and Their Influence on Exciton Relaxation Pathways. *ACS Nano* **2014,** *8*, 2512-2521.

19. Owen, J., The Coordination Chemistry of Nanocrystal Surfaces. *Science* **2015,** *347*, 615-616.

20. Zhou, T.; Anderson, R. T.; Li, H.; Bell, J.; Yang, Y.; Gorman, B. P.; Pylypenko, S.; Lusk, M. T.; Sellinger, A., Bandgap Tuning of Silicon Quantum Dots by Surface Functionalization with Conjugated Organic Groups. *Nano Lett.* **2015,** *15*, 3657-3663.

21. Knauf, R. R.; Lennox, J. C.; Dempsey, J. L., Quantifying Ligand Exchange Reactions at CdSe Nanocrystal Surfaces. *Chem. Mater.* **2016,** *28*, 4762-4770.

22. Alivisatos, A. P., Perspectives on the Physical Chemistry of Semiconductor Nanocrystals. *J. Phys. Chem.* **1996,** *100*, 13226-13239.

23. El-Sayed, M. A., Small is Different: Shape-, Size-, and Composition-Dependent Properties of Some Colloidal Semiconductor Nanocrystals. *Acc. Chem. Res.* **2004,** *37*, 326-333.

24. Guo, Y. J.; Alvarado, S. R.; Barclay, J. D.; Vela, J., Shape-Programmed Nanofabrication: Understanding the Reactivity of Dichalcogenide Precursors. *ACS Nano* **2013,** *7*, 3616-3626.

25. Levchenko, T. I.; Kubel, C.; Najafabadi, B. K.; Boyle, P. D.; Cadogan, C.; Goncharova, L. V.; Garreau, A.; Lagugne-Labarthet, F.; Huang, Y. N.; Corrigan, J. F., Luminescent CdSe Superstructures: A Nanocluster Superlattice and a Nanoporous Crystal. *J. Am. Chem. Soc.* **2017,** *139*, 1129-1144.

26. Thayer, A. M.; Steigerwald, M. L.; Duncan, T. M.; Douglass, D. C., NMR Study of Semiconductor Molecular Clusters. *Phys. Rev. Lett.* **1988,** *60*, 2673-2676.

27. Ladizhansky, V.; Hodes, G.; Vega, S., Surface Properties of Precipitated CdS Nanoparticles Studied by NMR. *J. Phys. Chem. B* **1998,** *102*, 8505-8509.

28. Berrettini, M. G.; Braun, G.; Hu, J. G.; Strouse, G. F., NMR Analysis of Surfaces and Interfaces in 2-nm CdSe. *J. Am. Chem. Soc.* **2004,** *126*, 7063-7070.

29. Ratcliffe, C. I.; Yu, K.; Ripmeester, J. A.; Zaman, M. B.; Badarau, C.; Singh, S., Solid State NMR Studies of Photoluminescent Cadmium Chalcogenide Nanoparticles. *Phys. Chem. Chem. Phys.* **2006,** *8*, 3510-3519.

30. Wang, R.; Calvignanello, O.; Ratcliffe, C. I.; Wu, X.; Leek, D. M.; Zaman, M. B.; Kingston, D.; Ripmeester, J. A.; Yu, K., Homogeneously-Alloyed CdTeSe Single-Sized Nanocrystals with Bandgap Photoluminescence. *J. Phys. Chem. C* **2009,** *113*, 3402-3408.

31. Lovingood, D. D.; Achey, R.; Paravastu, A. K.; Strouse, G. F., Size- and Site-Dependent Reconstruction in CdSe QDs Evidenced by 77Se{1H} CP-MAS NMR Spectroscopy. *J. Am. Chem. Soc.* **2010,** *132*, 3344-3354.

32. Kurihara, T.; Noda, Y.; Takegoshi, K., Quantitative Solid-State NMR Study on Ligand-Surface Interaction in Cysteine-Capped CdSe Magic-Sized Clusters. *J. Phys. Chem. Lett.* **2017**, 2555-2559.

33. Levchenko, T. I.; Lucier, B. E. G.; Corrigan, J. F.; Huang, Y., Crystalline Superlattices of Nanoscopic CdS Molecular Clusters: An X-ray Crystallography and ^{111}Cd SSNMR Spectroscopy Study. *Inorg. Chem.* **2018,** *57*, 204-217.

34. Kurihara, T.; Noda, Y.; Takegoshi, K., Capping Structure of Ligand-Cysteine on CdSe Magic-Sized Clusters. *ACS Omega* **2019,** *4*, 3476-3483.

35. Tomaselli, M.; Yarger, J. L.; Bruchez, M.; Havlin, R. H.; deGraw, D.; Pines, A.; Alivisatos, A. P., NMR Study of InP Quantum Dots: Surface Structure and Size Effects. *J. Chem. Phys.* **1999,** *110*, 8861-8864.

36. Cros-Gagneux, A.; Delpech, F.; Nayral, C.; Cornejo, A.; Coppel, Y.; Chaudret, B., Surface Chemistry of InP Quantum Dots: A Comprehensive Study. *J. Am. Chem. Soc.* **2010,** *132*, 18147-18157.

37. Virieux, H.; Le Troedec, M.; Cros-Gagneux, A.; Ojo, W. S.; Delpech, F.; Nayral, C.; Martinez, H.; Chaudret, B., InP/ZnS Nanocrystals: Coupling NMR and XPS for Fine Surface and Interface Description. *J. Am. Chem. Soc.* **2012,** *134*, 19701-19708.

38. Carter, R. S.; Harley, S. J.; Power, P. P.; Augustine, M. P., Use of NMR Spectroscopy in the Synthesis and Characterization of Air-

and Water-Stable Silicon Nanoparticles from Porous Silicon. *Chem. Mater.* **2005,** *17*, 2932-2939.
39. Neiner, D.; Kauzlarich, S. M., Hydrogen-Capped Silicon Nanoparticles as a Potential Hydrogen Storage Material: Synthesis, Characterization, and Hydrogen Release. *Chem. Mater.* **2010,** *22*, 487-493.
40. Lee, D.; Kaushik, M.; Coustel, R.; Chenavier, Y.; Chanal, M.; Bardet, M.; Dubois, L.; Okuno, H.; Rochat, N.; Duclairoir, F.; Mouesca, J. M.; De Paepe, G., Solid-State NMR and DFT Combined for the Surface Study of Functionalized Silicon Nanoparticles. *Chem. Eur. J.* **2015,** *21*, 16047-16058.
41. Hanrahan, M. P.; Fought, E. L.; Windus, T. L.; Wheeler, L. M.; Anderson, N. C.; Neale, N. R.; Rossini, A. J., Characterization of Silicon Nanocrystal Surfaces by Multidimensional Solid-State NMR Spectroscopy. *Chem. Mater.* **2017,** *29*, 10339-10351.
42. Thiessen, A. N.; Ha, M.; Hooper, R. W.; Yu, H.; Oliynyk, A. O.; Veinot, J. G. C.; Michaelis, V. K., Silicon Nanoparticles: Are They Crystalline from the Core to the Surface? *Chem. Mater.* **2019,** *31*, 678-688.
43. Cadars, S.; Smith, B. J.; Epping, J. D.; Acharya, S.; Belman, N.; Golan, Y.; Chmelka, B. F., Atomic Positional Versus Electronic Order in Semiconducting ZnSe Nanoparticles. *Phys. Rev. Lett.* **2009,** *103*, 136802.
44. Wang, R.; Ratcliffe, C. I.; Wu, X.; Voznyy, O.; Tao, Y.; Yu, K., Magic-Sized Cd_3P_2 II−V Nanoparticles Exhibiting Bandgap Photoemission. *J. Phys. Chem. C* **2009,** *113*, 17979-17982.
45. Yesinowski, J. P., Solid-State NMR of Inorganic Semiconductors. In *Solid State NMR*, Chan, J. C. C., Ed. Springer Berlin Heidelberg: Berlin, Heidelberg, 2012; pp 229-312.
46. Yesinowski, J. P.; Berkson, Z. J.; Cadars, S.; Purdy, A. P.; Chmelka, B. F., Spatially Correlated Distributions of Local Metallic Properties in Bulk and Nanocrystalline GaN. *Phys. Rev. B* **2017,** *95*, 235201.
47. Maciel, G. E.; Sindorf, D. W., Silicon-29 Nuclear Magnetic Resonance Study of the Surface of Silica-Gel by Cross Polarization and Magic Angle Spinning. *J. Am. Chem. Soc.* **1980,** *102*, 7606-7607.
48. Sindorf, D. W.; Maciel, G. E., Si-29 NMR-Study of Dehydrated Rehydrated Silica-Gel Using Cross Polarization and Magic-Angle Spinning. *J. Am. Chem. Soc.* **1983,** *105*, 1487-1493.
49. Morris, H. D.; Ellis, P. D., ^{27}Al Cross Polarization of Aluminas. The NMR Spectroscopy of Surface Aluminum Atoms. *J. Am. Chem. Soc.* **1989,** *111*, 6045-6049.
50. Lesage, A.; Lelli, M.; Gajan, D.; Caporini, M. A.; Vitzthum, V.; Miéville, P.; Alauzun, J.; Roussey, A.; Thieuleux, C.; Mehdi, A.; Bodenhausen, G.; Coperet, C.; Emsley, L., Surface Enhanced NMR Spectroscopy by Dynamic Nuclear Polarization. *J. Am. Chem. Soc.* **2010,** *132*, 15459-15461.
51. Lee, D.; Duong, N. T.; Lafon, O.; De Paepe, G., Primostrato Solid-State NMR Enhanced by Dynamic Nuclear Polarization: Pentacoordinated Al^{3+} Ions Are Only Located at the Surface of Hydrated γ-Alumina. *J. Phys. Chem. C* **2014,** *118*, 25065-25076.
52. Piveteau, L.; Ong, T. C.; Rossini, A. J.; Emsley, L.; Coperet, C.; Kovalenko, M. V., Structure of Colloidal Quantum Dots from Dynamic Nuclear Polarization Surface Enhanced NMR Spectroscopy. *J. Am. Chem. Soc.* **2015,** *137*, 13964-13971.
53. Pines, A., Proton-Enhanced NMR of Dilute Spins in Solids. *J. Chem. Phys.* **1973,** *59*, 569-590.
54. Lelli, M.; Gajan, D.; Lesage, A.; Caporini, M. A.; Vitzthum, V.; Mieville, P.; Heroguel, F.; Rascon, F.; Roussey, A.; Thieuleux, C.; Boualleg, M.; Veyre, L.; Bodenhausen, G.; Coperet, C.; Emsley, L., Fast Characterization of Functionalized Silica Materials by Silicon-29 Surface-Enhanced NMR Spectroscopy Using Dynamic Nuclear Polarization. *J. Am. Chem. Soc.* **2011,** *133*, 2104-2107.
55. Piveteau, L.; Ong, T.-C.; Walder, B. J.; Dirin, D. N.; Moscheni, D.; Schneider, B.; Bär, J.; Protesescu, L.; Masciocchi, N.; Guagliardi, A.; Emsley, L.; Copéret, C.; Kovalenko, M. V., Resolving the Core and the Surface of CdSe Quantum Dots and Nanoplatelets Using Dynamic Nuclear Polarization Enhanced PASS–PIETA NMR Spectroscopy. *ACS Cent. Sci.* **2018,** *4*, 1113-1125.
56. Mazoyer, E.; Trebosc, J.; Baudouin, A.; Boyron, O.; Pelletier, J.; Basset, J. M.; Vitorino, M. J.; Nicholas, C. P.; Gauvin, R. M.; Taoufik, M.; Delevoye, L., Heteronuclear NMR Correlations To Probe the Local Structure of Catalytically Active Surface Aluminum Hydride Species on γ-Alumina. *Angew. Chem. Int. Ed.* **2010,** *49*, 9854-9858.
57. Maly, T.; Debelouchina, G. T.; Bajaj, V. S.; Hu, K. N.; Joo, C. G.; Mak-Jurkauskas, M. L.; Sirigiri, J. R.; van der Wel, P. C. A.; Herzfeld, J.; Temkin, R. J.; Griffin, R. G., Dynamic Nuclear Polarization at High Magnetic Fields. *J. Chem. Phys.* **2008,** *128*, 052211.
58. Rosay, M.; Tometich, L.; Pawsey, S.; Bader, R.; Schauwecker, R.; Blank, M.; Borchard, P. M.; Cauffman, S. R.; Felch, K. L.; Weber, R. T.; Temkin, R. J.; Griffin, R. G.; Maas, W. E., Solid-State Dynamic Nuclear Polarization at 263 GHz: Spectrometer Design and Experimental Results. *Phys. Chem. Chem. Phys.* **2010,** *12*, 5850-5860.
59. Ni, Q. Z.; Daviso, E.; Can, T. V.; Markhasin, E.; Jawla, S. K.; Swager, T. M.; Temkin, R. J.; Herzfeld, J.; Griffin, R. G., High Frequency Dynamic Nuclear Polarization. *Acc. Chem. Res.* **2013,** *46*, 1933-1941.
60. Lilly Thankamony, A. S.; Wittmann, J. J.; Kaushik, M.; Corzilius, B., Dynamic Nuclear Polarization for Sensitivity Enhancement in Modern Solid-State NMR. *Prog. Nucl. Magn. Reson. Spectrosc.* **2017,** *102-103*, 120-195.
61. Rossini, A. J.; Zagdoun, A.; Lelli, M.; Lesage, A.; Coperet, C.; Emsley, L., Dynamic Nuclear Polarization Surface Enhanced NMR Spectroscopy. *Acc. Chem. Res.* **2013,** *46*, 1942-1951.
62. Maly, T.; Andreas, L. B.; Smith, A. A.; Griffin, R. G., H-2-DNP-Enhanced H-2-C-13 Solid-State NMR Correlation Spectroscopy. *Phys. Chem. Chem. Phys.* **2010,** *12*, 5872-5878.
63. Mehler, M.; Eckert, C. E.; Leeder, A. J.; Kaur, J.; Fischer, T.; Kubatova, N.; Brown, L. J.; Brown, R. C. D.; Becker-Baldus, J.; Wachtveitl, J.; Glaubitz, C., Chromophore Distortions in Photointermediates of Proteorhodopsin visualized by DNP-enhanced solid-state NMR. *J. Am. Chem. Soc.* **2017,** *139*, 16143-16153.
64. Zhao, L.; Pinon, A. C.; Emsley, L.; Rossini, A. J., DNP-Enhanced Solid-State NMR Spectroscopy of Active Pharmaceutical Ingredients. *Magn. Reson. Chem.* **2018,** *56*, 583-609.
65. Blanc, F.; Chong, S. Y.; McDonald, T. O.; Adams, D. J.; Pawsey, S.; Caporini, M. A.; Cooper, A. I., Dynamic Nuclear Polarization NMR Spectroscopy Allows High-Throughput Characterization of Microporous Organic Polymers. *J. Am. Chem. Soc.* **2013,** *135*, 15290-15293.
66. Eedugurala, N.; Wang, Z.; Chaudhary, U.; Nelson, N.; Kandel, K.; Kobayashi, T.; Slowing, I. I.; Pruski, M.; Sadow, A. D., Mesoporous Silica-Supported Amidozirconium-Catalyzed Carbonyl Hydroboration. *ACS Catal.* **2015,** *5*, 7399-7414.
67. Berruyer, P.; Lelli, M.; Conley, M. P.; Silverio, D. L.; Widdifield, C. M.; Siddiqi, G.; Gajan, D.; Lesage, A.; Coperet, C.; Emsley, L., Three-Dimensional Structure Determination of Surface Sites. *J. Am. Chem. Soc.* **2017,** *139*, 849-855.
68. Perras, F. A.; Padmos, J. D.; Johnson, R. L.; Wang, L.-L.; Schwartz, T. J.; Kobayashi, T.; Horton, J. H.; Dumesic, J. A.; Shanks, B. H.; Johnson, D. D.; Pruski, M., Characterizing Substrate–Surface Interactions on Alumina-Supported Metal Catalysts by Dynamic Nuclear Polarization-Enhanced Double-Resonance NMR Spectroscopy. *J. Am. Chem. Soc.* **2017,** *139*, 2702-2709.
69. Blanc, F.; Sperrin, L.; Lee, D.; Dervisoglu, R.; Yamazaki, Y.; Haile, S. M.; De Paepe, G.; Grey, C. P., Dynamic Nuclear Polarization NMR of Low-γ Nuclei: Structural Insights into Hydrated Yttrium-Doped $BaZrO_3$. *J. Phys. Chem. Lett.* **2014,** *5*, 2431-2436.
70. Bjorgvinsdottir, S.; Walder, B. J.; Pinon, A. C.; Emsley, L., Bulk Nuclear Hyperpolarization of Inorganic Solids by Relay from the Surface. *J. Am. Chem. Soc.* **2018,** *140*, 7946-7951.
71. Wolf, T.; Kumar, S.; Singh, H.; Chakrabarty, T.; Aussenac, F.; Frenkel, A. I.; Major, D. T.; Leskes, M., Endogenous Dynamic Nuclear Polarization for Natural Abundance ^{17}O and Lithium NMR in the Bulk of Inorganic Solids. *J. Am. Chem. Soc.* **2019,** *141*, 451-462.
72. Jin, Y. T.; Kneusels, N. J. H.; Marbella, L. E.; Castillo-Martinez, E.; Magusin, P. C. M. M.; Weatherup, R. S.; Jonsson, E.; Liu, T.; Paul, S.; Grey, C. P., Understanding Fluoroethylene Carbonate and Vinylene Carbonate Based Electrolytes for Si Anodes in Lithium Ion Batteries with NMR Spectroscopy. *J. Am. Chem. Soc.* **2018,** *140*, 9854-9867.
73. Lafon, O.; Rosay, M.; Aussenac, F.; Lu, X.; Trébosc, J.; Cristini, O.; Kinowski, C.; Touati, N.; Vezin, H.; Amoureux, J.-P., Beyond the Silica Surface by Direct Silicon-29 Dynamic Nuclear Polarization. *Angew. Chem. Int. Ed.* **2011,** *50*, 8367-8370.
74. Vitzthum, V.; Mieville, P.; Carnevale, D.; Caporini, M. A.; Gajan, D.; Coperet, C.; Lelli, M.; Zagdoun, A.; Rossini, A. J.; Lesage, A.; Emsley, L.; Bodenhausen, G., Dynamic Nuclear Polarization of

Quadrupolar Nuclei using Cross Polarization from Protons: Surface-Enhanced Aluminium-27 NMR. *Chem. Commun.* **2012,** *48*, 1988-1990.

75. Lafon, O.; Thankamony, A. S. L.; Kobayashi, T.; Carnevale, D.; Vitzthum, V.; Slowing, I. I.; Kandel, K.; Vezin, H.; Amoureux, J. P.; Bodenhausen, G.; Pruski, M., Mesoporous Silica Nanoparticles Loaded with Surfactant: Low Temperature Magic Angle Spinning ^{13}C and ^{29}Si NMR Enhanced by Dynamic Nuclear Polarization. *J. Phys. Chem. C* **2013,** *117*, 1375-1382.

76. Protesescu, L.; Rossini, A. J.; Kriegner, D.; Valla, M.; de Kergommeaux, A.; Walter, M.; Kravchyk, K. V.; Nachtegaal, M.; Stangl, J.; Malaman, B.; Reiss, P.; Lesage, A.; Emsley, L.; Coperet, C.; Kovalenko, M. V., Unraveling the Core-Shell Structure of Ligand-Capped Sn/SnO_x Nanoparticles by Surface-Enhanced Nuclear Magnetic Resonance, Mossbauer, and X-ray Absorption Spectroscopies. *ACS Nano* **2014,** *8*, 2639-2648.

77. Presti, C.; Thankamony, A. S. L.; Alauzun, J. G.; Mutin, P. H.; Carnevale, D.; Lion, C.; Vezin, H.; Laurencin, D.; Lafon, O., NMR and EPR Characterization of Functionalized Nanodiamonds. *J. Phys. Chem. C* **2015,** *119*, 12408-12422.

78. Hope, M. A.; Halat, D. M.; Magusin, P. C.; Paul, S.; Peng, L.; Grey, C. P., Surface-Selective Direct ^{17}O DNP NMR of CeO_2 Nanoparticles. *Chem. Commun.* **2017,** *53*, 2142-2145.

79. Viger-Gravel, J.; Berruyer, P.; Gajan, D.; Basset, J. M.; Lesage, A.; Tordo, P.; Ouari, O.; Emsley, L., Frozen Acrylamide Gels as Dynamic Nuclear Polarization Matrices. *Angew. Chem. Int. Ed.* **2017,** *56*, 8726-8730.

80. Ha, M.; Thiessen, A. N.; Sergeyev, I. V.; Veinot, J. G. C.; Michaelis, V. K., Endogenous Dynamic Nuclear Polarization NMR of Hydride-Terminated Silicon Nanoparticles. *Solid State Nucl. Magn. Reson.* **2019,** *100*, 77-84.

81. Kobayashi, T.; Perras, F. A.; Slowing, I. I.; Sadow, A. D.; Pruski, M., Dynamic Nuclear Polarization Solid-State NMR in Heterogeneous Catalysis Research. *ACS Catal.* **2015,** *5*, 7055-7062.

82. Lafon, O.; Thankamony, A. S. L.; Rosay, M.; Aussenac, F.; Lu, X. Y.; Trebosc, J.; Bout-Roumazeilles, V.; Vezine, H.; Amoureux, J. P., Indirect and Direct ^{29}Si Dynamic Nuclear Polarization of Dispersed Nanoparticles. *Chem. Commun.* **2013,** *49*, 2864-2866.

83. Kubicki, D. J.; Rossini, A. J.; Purea, A.; Zagdoun, A.; Ouari, O.; Tordo, P.; Engelke, F.; Lesage, A.; Emsley, L., Amplifying Dynamic Nuclear Polarization of Frozen Solutions by Incorporating Dielectric Particles. *J. Am. Chem. Soc.* **2014,** *136*, 15711-8.

84. Lamb, J. W., Miscellaneous Data on Materials for Millimetre and Submillimetre Optics. *Int. J. Infared Millimeter Waves* **1996,** *17*, 1997-2034.

85. Kobayashi, T.; Singappuli-Arachchige, D.; Wang, Z. R.; Slowing, I. I.; Pruski, M., Spatial Distribution of Organic Functional Groups Supported on Mesoporous Silica Nanoparticles: a Study by Conventional and DNP-Enhanced ^{29}Si Solid-State NMR. *Phys. Chem. Chem. Phys.* **2017,** *19*, 1781-1789.

86. Mohandas, J. C.; Abou-Hamad, E.; Callens, E.; Samantaray, M. K.; Gajan, D.; Gurinov, A.; Ma, T.; Ould-Chikh, S.; Hoffman, A. S.; Gates, B. C.; Basset, J. M., From Single-Site Tantalum Complexes to Nanoparticles of Ta_xN_y and TaO_xN_y Supported on Silica: Elucidation of Synthesis Chemistry by Dynamic Nuclear Polarization Surface Enhanced NMR Spectroscopy and X-ray Absorption Spectroscopy. *Chem. Sci.* **2017,** *8*, 5650-5661.

87. Yu, W. W.; Qu, L. H.; Guo, W. Z.; Peng, X. G., Experimental Determination of the Extinction Coefficient of CdTe, CdSe, and CdS Nanocrystals. *Chem. Mater.* **2003,** *15*, 2854-2860.

88. Hassinen, A.; Moreels, I.; De Nolf, K.; Smet, P. F.; Martins, J. C.; Hens, Z., Short-Chain Alcohols Strip X-Type Ligands and Quench the Luminescence of PbSe and CdSe Quantum Dots, Acetonitrile Does Not. *J. Am. Chem. Soc.* **2012,** *134*, 20705-20712.

89. Hu, J. Z.; Wang, W.; Liu, F.; Solum, M. S.; Alderman, D. W.; Pugmire, R. J.; Grant, D. M., Magic-Angle-Turning Experiments for Measuring Chemical-Shift-Tensor Principal Values in Powdered Solids. *J. Magn. Reson., Ser. A* **1995,** *113*, 210-222.

90. Wolf, P.; Valla, M.; Rossini, A. J.; Comas-Vives, A.; Nunez-Zarur, F.; Malaman, B.; Lesage, A.; Emsley, L.; Coperet, C.; Hermans, I., NMR Signatures of the Active Sites in Sn-ß Zeolite. *Angew. Chem. Int. Ed.* **2014,** *53*, 10179-10183.

91. Nolle, A., Isotropic and Anisotropic Nuclear Magnetic Shielding of ^{113}Cd in Cadmiumhalides, Cadmiumchalcogenides and in Cadmiumcarbonate. *Z. Naturforsch., A: Phys. Sci.* **1978,** *33*, 666-671.

92. Lesage, A.; Auger, C.; Caldarelli, S.; Emsley, L., Determination of through-bond carbon-carbon connectivities in solid-state NMR using the INADEQUATE experiment. *J. Am. Chem. Soc.* **1997,** *119*, 7867-7868.

93. Dance, I. G.; Saunders, J. K., Cd-Cd Coupling in the ^{113}Cd-113 NMR Spectra (Including 2-Dimensional COSY) of Molecular Polycadmium Thiolate Aggregates. *Inorg. Chim. Acta* **1985,** *96*, L71-L73.

94. Schmidt-Rohr, K.; Clauss, J.; Spiess, H. W., Correlation of Structure, Mobility, and Morphological Information in Heterogeneous Polymer Materials by Two-Dimensional Wideline-Separation NMR-Spectroscopy. *Macromolecules* **1992,** *25*, 3273-3277.

95. Colombo, M. G.; Meier, B. H.; Ernst, R. R., Rotor-Driven Spin Diffusion in Natural-Abundance ^{13}C Spin Systems. *Chem. Phys. Lett.* **1988,** *146*, 189-196.

96. Kubo, A.; Mcdowell, C. A., Spectral Spin Diffusion in Polycrystalline Solids under Magic-Angle Spinning. *J. Chem. Soc., Faraday Trans. 1* **1988,** *84*, 3713-3730.

97. Challoner, R.; Kummerlen, J.; Mcdowell, C. A., Spectral Spin Diffusion under n=0 Rotational Resonance. *Mol. Phys.* **1994,** *83*, 687-700.

98. Miao, S. D.; Hickey, S. G.; Rellinghaus, B.; Waurisch, C.; Eychmuller, A., Synthesis and Characterization of Cadmium Phosphide Quantum Dots Emitting in the Visible Red to Near-Infrared. *J. Am. Chem. Soc.* **2010,** *132*, 5613-5615.

99. Ojo, W. S.; Xu, S.; Delpech, F.; Nayral, C.; Chaudret, B., Room-Temperature Synthesis of Air-Stable and Size-Tunable Luminescent ZnS-Coated Cd_3P_2 Nanocrystals with High Quantum Yields. *Angew. Chem. Int. Ed.* **2012,** *51*, 738-741.

100. Glassy, B. A.; Cossairt, B. M., II_3V_2 (II: Zn, Cd; V: P, As) Semiconductors: From Bulk Solids to Colloidal Nanocrystals. *Small* **2017,** *13*, 1702038.

101. Stein, J. L.; Holden, W. M.; Venkatesh, A.; Mundy, M. E.; Rossini, A. J.; Seidler, G. T.; Cossairt, B. M., Probing Surface Defects of InP Quantum Dots Using Phosphorus Kα and Kß X-ray Emission Spectroscopy. *Chem. Mater.* **2018,** *30*, 6377-6388.

102. Baquero, E. A.; Ojo, W. S.; Coppel, Y.; Chaudret, B.; Urbaszek, B.; Nayral, C.; Delpech, F., Identifying Short Surface Ligands on Metal Phosphide Quantum Dots. *Phys. Chem. Chem. Phys.* **2016,** *18*, 17330-17334.

103. Holl, S. M.; Kowalewski, T.; Schaefer, J., Characterization of Two Forms of Cadmium Phosphide by Magic-Angle Spinning ^{31}P NMR. *Solid State Nucl. Magn. Reson.* **1996,** *6*, 39-46.

104. Dixon, W. T.; Schaefer, J.; Sefcik, M. D.; Stejskal, E. O.; Mckay, R. A., Total Suppression of Sidebands in CPMAS C-13 NMR. *J. Magn. Reson.* **1982,** *49*, 341-345.

105. Bak, M.; Rasmussen, J. T.; Nielsen, N. C., SIMPSON: A General Simulation Program for Solid-State NMR Spectroscopy. *J. Magn. Reson.* **2000,** *147*, 296-330.

106. Tosner, Z.; Vosegaard, T.; Kehlet, C.; Khaneja, N.; Glaser, S. J.; Nielsen, N. C., Optimal Control in NMR Spectroscopy: Numerical Implementation in SIMPSON. *J. Magn. Reson.* **2009,** *197*, 120-134.

107. Tosner, Z.; Andersen, R.; Stevenss, B.; Eden, M.; Nielsen, N. C.; Vosegaard, T., Computer-Intensive Simulation of Solid-State NMR Experiments using SIMPSON. *J. Magn. Reson.* **2014,** *246*, 79-93.

108. Lee, D.; Monin, G.; Duong, N. T.; Lopez, I. Z.; Bardet, M.; Mareau, V.; Gonon, L.; De Paepe, G., Untangling the Condensation Network of Organosiloxanes on Nanoparticles Using 2D ^{29}Si-^{29}Si Solid-State NMR Enhanced by Dynamic Nuclear Polarization. *J. Am. Chem. Soc.* **2014,** *136*, 13781-8.

109. Hahn, J., Contributions to the Chemistry of Silicon and Germanium XXIX [1] Si-29 NMR Spectroscopic Investigations on Straight and Branched Silanes. *Z. Naturforsch., B: J. Chem. Sci.* **1980,** *35*, 282-296.

110. Stein, J. L.; Steimle, M. I.; Terban, M. W.; Petrone, A.; Billinge, S. J. L.; Li, X. S.; Cossairt, B. M., Cation Exchange Induced Transformation of InP Magic-Sized Clusters. *Chem. Mater.* **2017,** *29*, 7984-7992.

111. Wheeler, L. M.; Anderson, N. C.; Palomaki, P. K. B.; Blackburn, J. L.; Johnson, J. C.; Neale, N. R., Silyl Radical Abstraction in the Functionalization of Plasma-Synthesized Silicon Nanocrystals. *Chem. Mater.* **2015,** *27*, 6869-6878.

112. Carroll, G. M.; Limpens, R.; Neale, N. R., Tuning Confinement in Colloidal Silicon Nanocrystals with Saturated Surface Ligands. *Nano Lett.* **2018,** *18*, 3118-3124.
113. Harris, R. K.; Becker, E. D.; De Menezes, S. M. C.; Goodfellow, R.; Granger, P., NMR Nomenclature. Nuclear Spin Properties and Conventions for Chemical Shifts - (IUPAC Recommendations 2001). *Pure Appl. Chem.* **2001,** *73*, 1795-1818.
114. Trebosc, J.; Wiench, J. W.; Huh, S.; Lin, V. S. Y.; Pruski, M., Studies of Organically Functionalized Mesoporous Silicas Using Heteronuclear Solid-State Correlation NMR Spectroscopy Under Fast Magic Angle Spinning. *J. Am. Chem. Soc.* **2005,** *127*, 7587-7593.
115. Fyfe, C. A.; Mueller, K. T.; Grondey, H.; Wongmoon, K. C., Dipolar Dephasing between Quadrupolar and Spin-1/2 Nuclei. REDOR and TEDOR NMR Experiments on VPI-5. *Chem. Phys. Lett.* **1992,** *199*, 198-204.
116. Rossini, A. J.; Hanrahan, M. P.; Thuo, M., Rapid Acquisition of Wideline MAS Solid-State NMR Spectra with Fast MAS, Proton Detection, and Dipolar HMQC Pulse Sequences. *Phys. Chem. Chem. Phys.* **2016,** *18*, 25284-25295.
117. Gan, Z. H., $^{13}C/^{14}N$ Heteronuclear Multiple-Quantum Correlation with Rotary Resonance and REDOR Dipolar Recoupling. *J. Magn. Reson.* **2007,** *184*, 39-43.
118. Elena, B.; Lesage, A.; Steuernagel, S.; Bockmann, A.; Emsley, L., Proton to Carbon-13 INEPT in Solid-State NMR Spectroscopy. *Journal of the American Chemical Society* **2005,** *127*, 17296-17302.
119. Gullion, T.; Schaefer, J., Rotational-Echo Double-Resonance NMR. *J. Magn. Reson.* **1989,** *81*, 196-200.
120. Gullion, T.; Baker, D. B.; Conradi, M. S., New, Compensated Carr-Purcell Sequences. *J. Magn. Reson.* **1990,** *89*, 479-484.
121. Fung, B. M.; Khitrin, A. K.; Ermolaev, K., An Improved Broadband Decoupling Sequence for Liquid Crystals and Solids. *J. Magn. Reson.* **2000,** *142*, 97-101.

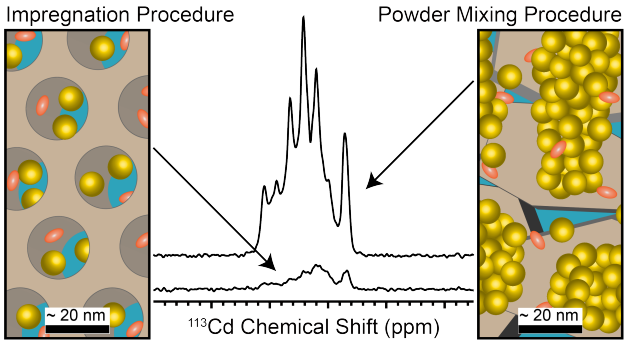
Impregnation Procedure
Powder Mixing Procedure
~ 20 nm
~ 20 nm
113Cd Chemical Shift (ppm)